

Charm Meson Decays

MARINA ARTUSO^a, BRIAN MEADOWS^b, ALEXEY A PETROV^{c,d}

^aSyracuse University, Syracuse, NY 13244, USA

^bUniversity of Cincinnati, Cincinnati, OH 45221, USA

^cWayne State University, Detroit, MI 48201, USA

^dMCTP, University of Michigan, Ann Arbor, MI 48109, USA

Key Words charmed quark, charmed meson, weak decays, CP-violation

Abstract We review some recent developments in charm meson physics. In particular, we discuss theoretical predictions and experimental measurements of charmed meson decays to leptonic, semileptonic, and hadronic final states and implications of such measurements to searches for new physics. We discuss $D^0 - \bar{D}^0$ -mixing and CP-violation in charm, and discuss future experimental prospects and theoretical challenges in this area.

CONTENTS

INTRODUCTION	2
LEPTONIC AND SEMILEPTONIC DECAYS	3
<i>Theoretical Predictions for the Decay Constant</i>	5
<i>Experimental Determinations of f_D</i>	5
<i>Constraints on New Physics from f_D</i>	6
<i>Absolute Branching Fractions for Semileptonic D Decays</i>	6
<i>Form Factors For The Decays $D \rightarrow K(\pi)\ell\nu$</i>	7
<i>The CKM Matrix</i>	9
<i>Form Factors in Semileptonic $D \rightarrow V\ell\nu$ Decays</i>	9
RARE AND RADIATIVE DECAYS	10
<i>Theoretical Motivation</i>	10
<i>Experimental Information</i>	12
HADRONIC DECAYS	13
<i>Theoretical Considerations</i>	13
<i>Branching Fraction Measurements</i>	14
<i>Three Body Decays</i>	16
CHARM MIXING AND CP-VIOLATION	21
<i>Charm mixing predictions in the Standard Model</i>	22
<i>New Physics contribution to $D^0 - \bar{D}^0$ mixing</i>	23
<i>CP-violation</i>	24
<i>Experimental Considerations</i>	26
<i>Experimental Studies of $D^0 - \bar{D}^0$ Mixing</i>	27
<i>Time-Dependent Studies</i>	27
<i>Time Independent Studies</i>	30

CONCLUSIONS AND OUTLOOK	32
ACKNOWLEDGMENTS	33

1 INTRODUCTION

The charm quark has played a unique role in particle physics for more than three decades. Its discovery by itself was an important validation of the Standard Model (SM), as its existence and mass scale were predicted (1) on the basis of low-energy kaon experiments before any direct experimental signature for charm was available.

Several features distinguish charmed hadrons from those with other flavors. While their mass, $\mathcal{O}(2 \text{ GeV})$ places them in the region where non-perturbative hadronic physics is operative, theoretical methods developed for heavy quarks can in principle still be applied, albeit with larger uncertainties. On the other hand, recent advances in unquenched lattice QCD simulations paved the way for charm data to be used to probe the Yukawa sector of the SM. It is the only up-type quark that can have flavor oscillations. Finally, charm decays provide a unique window on new physics (NP) affecting the up-type quark dynamics. In many cases, charm transitions provide almost background-free low-energy signals of NP. For example, many popular NP models predict signals for CP-violation (CPV) much larger than what is generally predicted within the SM (2). One hopes that, just like manifestation for charm quark existence came from low-energy kaon oscillation experiments, oscillations of charmed hadrons can provide hints of what is happening at the TeV scale.

Experiments operating at the $\psi(3770)$ resonance, near threshold for $D\bar{D}$ production, such as MARK III at SPEAR, performed the initial exploration of charm phenomenology (3). Later, higher energy machines, either fixed target experiments operating at hadron machines or higher energy e^+e^- colliders, entered this arena, with much bigger data samples. In recent years, we have seen a renewed interest in studying open charm in e^+e^- colliders with a center-of-mass energy close to $D\bar{D}$ threshold. The CLEO experiment(4) at CESR, after years of charm studies at a center-of-mass energy near the $\Upsilon(4S)$, has collected a sample exceeding 800 pb^{-1} at the $\psi(3770)$ center-of-mass energy, and a sample of about 600 pb^{-1} at a center-of-mass energy close to 4170 MeV , optimal for D_s studies. The BES-II experiment, at BEPC, has published results based on 33 pb^{-1} accumulated around the $\psi(3770)$. It has an upgrade program both for the detector (BESIII) and the machine (BEPICII), designed as a charm factory with $10^{33} \text{ cm}^{-2} \text{ s}^{-1}$ peak luminosity that should be completed in 2008 (5). In parallel, BABAR and Belle have provided important contributions to our knowledge of charm decays, exploiting their impressive data sets. Both B factory facilities have achieved luminosities almost ten times their original design. A KEK-B upgrade has been approved to attain luminosities about one order of magnitude greater than already achieved. An alternative approach, with higher luminosity goals and the added capability to run at both $\Upsilon(4S)$ and at the $\psi(3770)$, is being considered, but is not approved. Finally, CDF and D0 have entered the arena of charm physics, applying to this study some of the tools developed to pursue beauty physics.

Experiments operating at the $\psi(3770)$ resonance have several advantages: the final state is extremely simple, being dominated by a $D\bar{D}$ pair. The cross section

for charm production is relatively high, $\sigma(D^0\bar{D}^0) = 3.66 \pm 0.03 \pm 0.06$ nb and $\sigma(D^+D^-) = 2.91 \pm 0.03 \pm 0.05$ nb (6). In addition, the relatively high branching fractions to low multiplicity final states allow the use of tagged samples, where one D is fully reconstructed (tag) and the rest of the event recoiling against the tag is used to study specific signals. This technique is particularly useful to study leptonic and semileptonic events, as it allows a precise reconstruction of the neutrino 4-momentum, and of the invariant mass squared of the lepton-neutrino pair (q^2). In addition, the $D\bar{D}$ pairs are produced in a $C = -1$ state, and this quantum coherence allows unique probes of mixing and CPV . On the other hand the b-factory experiments, Belle and BaBar, can also be considered charm factories. At the $\Upsilon(4S)$ center-of-mass energy, $\sigma(b\bar{b}) \sim 1.1$ nb, while $\sigma(c\bar{c}) \sim 1.3$ nb. The background to be tackled is higher than at the lower energy, and neutrino and q^2 reconstruction in general are not as precise. Significant improvements are achieved, however, through the use of tagged samples (7), made possible by the impressive size of the data set accumulated: in January 2008 the samples are 484 fb^{-1} at BABAR and 763 fb^{-1} at Belle. Also, the energy at which they operate makes possible the production of charmed baryons and boosts the charm particles sufficiently so that time dependent measurements are possible.

Experiments at hadron machines have the advantage of much higher cross sections for charm and beauty production, at the expense of significant backgrounds. Luckily the relative long lifetime of charm hadrons (~ 1 ps), combined with the development of silicon micropattern detectors provides a unique and powerful signature of charm meson decays: the identification of detached secondary vertices. About 30 years after its initial inception (8), this technique is still being perfected, introducing vertex algorithms more and more sophisticated that provide charm and beauty event tagging almost in real time. This development has allowed fixed target experiments and the two Tevatron experiments, CDF and D0, to provide significant contributions to our knowledge of charm decays, with competitive limits on some rare decays and recent results in $D^0\bar{D}^0$ mixing. This work will be continued by LHCb, the first dedicated charm and beauty experiment at a hadron collider (LHC), that relies heavily on detached vertex criteria in early stages of its triggering process and is considering an upgrade that would include detached vertex criteria in the lowest trigger level (9).

2 LEPTONIC AND SEMILEPTONIC DECAYS

Charm leptonic and semileptonic decays are ideal laboratories to study non-perturbative QCD, and to determine important quark mixing parameters. In addition, they may provide additional constraints on physics beyond the SM.

In the SM semileptonic decays are described by an effective Hamiltonian

$$\mathcal{H} = \frac{G_F}{\sqrt{2}} V_{cq} L^\mu \bar{q} \Gamma_\mu c, \quad (1)$$

with L^μ being a leptonic current, G_F is a Fermi constant, and $\Gamma_\mu = \gamma_\mu (1 - \gamma_5)$. Theoretically, leptonic decays are the simplest to describe, as they only depend on a single non-perturbative parameter, the decay constant f_{D_q} ,

$$\langle 0 | \bar{q} \gamma^\mu \gamma_5 c | D_q \rangle = -i f_{D_q} p_D^\mu, \quad (2)$$

which parameterizes the amplitude of probability for the heavy and a light quark to “find each other” in a meson. Semileptonic decays are traditionally described

in terms of form factors cast as a function of q^2 , the invariant mass of the electron-neutrino pair. Experimental determinations of these form factors are performed through the study of the differential decay width $d\Gamma/dq^2$. In both cases, decay constants and form factors are QCD parameters that can only be computed using non-perturbative techniques.

Accurate calculations of non-perturbative QCD parameters are very challenging. Lattice QCD represents an appealing approach. In principle, it is the only one that can be improved in a systematic way. A big stumbling block has been the inclusion of dynamical quark effects (unquenched lattice QCD). Recently, technical developments such as highly improved actions of QCD and the availability of “2+1 flavor” MILC configurations with 3 flavors of improved staggered quarks have lead to results with much higher accuracy and allowed for consistent estimate of both statistical and systematic errors involved in the simulations. Two groups have reported charm decay constant calculations with three dynamical quark flavors: the Fermilab/MILC Lattice collaboration (10) and the HPQCD collaboration (11). They both use the “2+1” MILC configurations including three flavors of staggered quarks: one heavier with a mass close to the strange quark mass m_s , and two degenerated light quarks with masses between $m_s/10$ and m_s , but differ on how they treat heavy quarks in their formulations of lattice QCD. The Fermilab group has also calculated the shape and normalization of the form factors in semileptonic $D \rightarrow \pi e \nu_e$ and $D \rightarrow K e \nu_e$ decays (12).

The QCD sum rules (13,14) provide a method for calculating hadronic matrix elements including non-perturbative effects that was designed to make maximum use of the known manifestations of non-perturbative QCD. A few parameters describe the non-perturbative dynamics and are fixed from well known hadronic processes, and then applied to heavy meson decays. Finally, quark models, generally QCD inspired and based on a variety of assumptions, have been used to predict form factor normalizations and decay constants (16).

In principle, charm meson semileptonic decays provide the simplest way to determine the magnitude of quark mixing parameters: the charm sector allows direct access to $|V_{cs}|$ and $|V_{cd}|$. Semileptonic decay rates are related to $|V_{cq}|^2$ via matrix elements that describe strong interaction effects.

The study of charm semileptonic decays may contribute to a precise determination of the Cabibbo Kobayashi Maskawa (*CKM*) matrix element $|V_{ub}|$. A variety of theoretical approaches have been proposed to use constraints provided by charm decays to reduce the model dependence in the extraction of $|V_{ub}|$ from exclusive charmless B semileptonic decays. In particular, if heavy quark effective theory (HQET) (17) is applicable both to the c and b quarks, there is an $SU(2)$ flavor symmetry that relates the form factors in D and B semileptonic decays (18). For example, a flavor symmetry relates the form factors in $D \rightarrow \pi \ell \nu$ are related to the ones in $B \rightarrow \pi \ell \bar{\nu}$, at the same $E \equiv v \cdot p_\pi$, where E is the energy of the light meson in the center-of-mass D frame, v is the four-velocity of the D meson, and p_P is the 4-momentum of the light hadron. The original method has been further refined (19); the large statistics needed to implement these methods may be available in the near future.

2.1 Theoretical Predictions for the Decay Constant

The leptonic decay width is given by

$$\Gamma(D_q \rightarrow \ell\nu) = \frac{G_F^2}{8\pi} f_{D_q}^2 m_\ell^2 M_{D_q} \left(1 - \frac{m_\ell^2}{M_{D_q}^2}\right)^2 |V_{cq}|^2, \quad (3)$$

where $q = d, s$ for D^+ or D_s states respectively, M_{D_q} is the D_q mass, m_ℓ is the mass of the final state lepton, and $|V_{cq}|$ is the CKM matrix element associated with the $c \rightarrow q$ transition. Due to helicity suppression, the rate goes as m_ℓ^2 ; consequently the electron mode $D^+ \rightarrow e^+\nu_e$ has a very small rate in the SM. The relative widths scale as $2.65 : 1 : 2.3 \times 10^{-5}$ for the $\tau^+\nu_\tau$, $\mu^+\nu_\mu$ and $e^+\nu_e$ final states, respectively. The decay constant f_D parameterizes a matrix element of the axial current and is the only non-perturbative parameter in Eq. (3). It can be related to the wave function overlap of charm quark and light antiquark. Charm meson decay constants are amenable to experimental and theory determination both for D^+ and D_s , thus allowing a direct measurement of $SU(3)$ breaking and a comparison with the theory.

2.2 Experimental Determinations of f_D

The CLEO collaboration (27) has measured $f_{D^+} = (222.6 \pm 16.7_{-3.4}^{+2.8})$ MeV, using a tagged sample of D^+D^- decays collected at a center-of-mass energy close to 3.77 GeV. The existence of the neutrino is inferred by requiring the missing mass squared (MM^2) to be consistent with zero,

$$MM^2 = (E_{beam} - E_{\mu^+})^2 - (\vec{p}_{D^-} - \vec{p}_{\mu^+})^2,$$

Figure 1 shows the measured MM^2 , with a 50 event peak in the interval $[-0.050 \text{ GeV}^2, +0.050 \text{ GeV}^2]$, approximately $\pm 2\sigma$ wide. The background is evaluated as $2.81 \pm 0.30 \pm 0.27$ events. The same tag sample is used to search for $D^+ \rightarrow e^+\nu_e$. No signal is found, corresponding to a 90% CL upper limit $\mathcal{B}(D^+ \rightarrow e^+\nu_e) < 2.4 \times 10^{-5}$. More data is available on $f_{D_s^+}$. Early measurements and a recent BaBar result of $f_{D_s^+}$ determine the ratio $\mathcal{B}(D_s \rightarrow \mu\nu)/\mathcal{B}(D_s \rightarrow \phi\pi)$ (28). This adds an additional large source of error as the denominator is not well known (33). CLEO-c uses a sample of $D_s D_s^*$ collected near the center-of-mass energy of 4.17 GeV to study D_s leptonic decays (34). They measure the branching fraction for the decays $D_s \rightarrow \mu\nu_\mu$, $D_s \rightarrow \tau\nu_\tau$, with $\tau \rightarrow \pi\nu_\tau$, and $\tau \rightarrow e\nu_\tau\nu_e$ (35). Recently, Belle has reported an absolute value for the branching fraction $\mathcal{B}(D_s \rightarrow \mu\nu_\mu)$ based on fully reconstructed samples of events of the type $e^+e^- \rightarrow D_s^* DKX$, $D_s^* \rightarrow D_s\gamma$ where X is any number of π and at most one γ from fragmentation (36). Theoretical predictions are summarized in Table 1, while measurements are shown in Table 2. The average of the absolute measurements is $f_{D_s^+} = 275 \pm 10$ MeV, assuming that $|V_{cs}| = |V_{cd}| = 0.9737$. Typically, the experimental value is above theoretical predictions. In general, the errors are such that the discrepancy is not yet meaningful, with the exception of the most recent UKQCD-MILC calculation (11). In this case, the discrepancy between theory and experiment exceeds their stated errors by about 3σ .

2.3 Constraints on New Physics from f_D

Leptonic decays are sensitive probes of NP interactions mediated by charged particles. Models with an extended Higgs sector, which include new charged scalar states, or models with broken left-right symmetry, which include massive vector W_R^\pm states, are primary examples of such interactions. Recent evidence of observation of $B \rightarrow \tau\nu_\tau$ decay brought renewed attention to such models. In particular, two Higgs doublet models, including Minimal Supersymmetric SM (MSSM), could give contributions to such transitions. Different implementations of this extension of the SM can be formulated (29). For example, the first doublet (Φ_1) could give mass to the up-type fermions and the second (Φ_2) to the down-type fermions. In this case,

$$\begin{aligned} \mathcal{B}(D^+ \rightarrow \ell^+ \nu_\ell) &= \mathcal{B}_{SM} \left(1 + \frac{m_D^2}{m_{H^\pm}^2} \right)^2 \\ \mathcal{B}(D_s^+ \rightarrow \ell^+ \nu_\ell) &= \mathcal{B}_{SM} \left[1 + \frac{m_{D_s}^2}{m_{H^\pm}^2} \left(1 - \tan^2 \beta \frac{m_s}{m_c} \right) \right]^2 \end{aligned} \quad (4)$$

Note that the latter model introduces a correction to the SM expectations that may be considerable and negative at large $\tan^2 \beta$. A limit can also be set on the mass of a charged Higgs, $m_{H^\pm} > 2.2 \tan \beta$. This limit is similar to the one obtained from the measurement $\mathcal{B}(B \rightarrow \tau\nu)$ decay (30).

2.4 Absolute Branching Fractions for Semileptonic D Decays

Determination of absolute branching fractions for D semileptonic decays constitute important measurements. Assuming $|V_{cx}|$ to be known, they determine form factor normalization. Conversely, if the form factors are known independently, say, from the lattice QCD calculations, these branching determine the relevant CKM matrix elements. By comparing the inclusive branching fractions of the D^+ and D^0 mesons with the sum of the measured exclusive branching fractions, one can determine whether there are semileptonic decay modes as yet unobserved. BES-II(32) and CLEO-c(31) have recently presented data on exclusive semileptonic branching fractions. BES-II results are based on 33 pb^{-1} ; CLEO-c's results are based on the first 57 pb^{-1} data set. Both experiments use tagged samples and select a specific final state through the kinematic variable:

$$U \equiv E_{miss} - |c\vec{p}_{miss}|,$$

where E_{miss} represents the missing energy and \vec{p} represents the missing momentum of the D meson decaying semileptonically. For signal events, U is expected to be 0, while other semileptonic decays peak in different regions. Fig. 2 shows the U distribution for 5 exclusive D^+ decay modes reported by CLEO-c, which demonstrate that U resolution is excellent, thus allowing a full separation between Cabibbo suppressed and Cabibbo favored modes. Table 3 summarizes the recent measurements from CLEO-c and BES-II, as well world averages reported in the Review of Particle Physics (33).

Absolute branching fractions for $D^0 \rightarrow K\ell\nu$ have been recently published by Belle (7): they obtain $\mathcal{B}(D^0 \rightarrow K\ell\nu) = (3.45 \pm 0.07 \pm 0.20)\%$ and $\mathcal{B}(D^0 \rightarrow \pi\ell\nu) = (0.255 \pm 0.019 \pm 0.016)\%$. CLEO-c uses the two tagging modes with

lowest background ($\bar{D}^0 \rightarrow K^+\pi^-$ and $D^- \rightarrow K^+\pi^-\pi^-$) to measure the inclusive D^0 and D^+ semileptonic branching fractions (42). They obtain

$$\mathcal{B}(D^+ \rightarrow Xe^+\nu_e) = (16.13 \pm 0.20_{\text{stat}} \pm 0.33_{\text{sys}})\%,$$

$$\mathcal{B}(D^0 \rightarrow Xe^+\nu_e) = (6.46 \pm 0.17_{\text{stat}} \pm 0.13_{\text{sys}})\%.$$

The sum of the exclusive semileptonic absolute branching fraction is $\mathcal{B}(D^+ \rightarrow Xe^+\nu_e)_{\text{excl}} = (15.1 \pm 0.5 \pm 0.5)\%$ and $\mathcal{B}(D^0 \rightarrow Xe^+\nu_e)_{\text{excl}} = (6.1 \pm 0.2 \pm 0.2)\%$: the measured exclusive modes are consistent with saturating the inclusive widths, although there is some room left for higher multiplicity modes. The CLEO-c data have been used in this comparison, as they dominate the present world average: the exclusive modes are consistent with saturating the inclusive semileptonic branching fraction at a 41% confidence level in the case of the D^+ and 18% confidence level in the case of the D^0 .

2.5 Form Factors For The Decays $D \rightarrow K(\pi)\ell\nu$

Theoretical parameterizations of semileptonic decays involve two non-perturbative quantities parameterizing matrix element of a single hadronic current. Traditionally, the hadronic matrix elements for transitions to pseudoscalar hadrons are described in terms of two form factors, $f_+(q^2)$ and $f_-(q^2)$,

$$\langle K(\pi) | \bar{q}\Gamma^\mu c | D \rangle = f_+(q^2)P^\mu + f_-(q^2)q^\mu, \quad (5)$$

where $P = p_D + p_{K(\pi)}$ and $q = p_D - p_{K(\pi)}$. An alternative parameterization is also often used,

$$\langle K(\pi) | \bar{q}\Gamma^\mu c | D \rangle = \left(P^\mu - \frac{m_D^2 - m_{K(\pi)}^2}{q^2} q^\mu \right) f_+(q^2) + \frac{m_D^2 - m_{K(\pi)}^2}{q^2} q^\mu f_0(q^2), \quad (6)$$

with $f_0(q^2) = f_+(q^2) + f_-(q^2)q^2/(m_D^2 - m_{K(\pi)}^2)$. Experimental determinations of these form factors are performed through the study of the differential decay width $d\Gamma/dq^2$. For cases where the lepton in the final state is an electron and has a negligible mass with respect to the parent D , only a single form factor, $f_+(q^2)$, contributes. The partial decay width is given by

$$\frac{d\Gamma(D \rightarrow K(\pi)e\nu_e)}{dq^2} = \frac{G_F^2 |V_{cq}|^2}{24\pi^3} p_{K(\pi)}^3 |f_+(q^2)|^2 \quad (7)$$

where $p_{K(\pi)}$ the hadron momentum in the D rest frame. Form factors have been evaluated at specific q^2 points in a variety of phenomenological models (43), where the shape is typically assumed from some model arguments. In order to restrict the function space studied, a dispersive representation (44) allows to place rather general constraints on the shapes of the form factors from their analytic properties. Particular parameterizations of the form factors are nevertheless useful. The most common parametrization has been a single pole form factor, where the pole is the lowest mass resonance formed by the initial and final state hadron. For example, in the decay $D \rightarrow \pi e \nu_e$ the dominant pole is the D^* . Now that more precise data are available, more complex representations are investigated.

One class of parameterizations include the dominant pole form factor and approximates the dispersion integral by a number of effective poles

$$f_+(q^2) = \frac{f_+(0)}{(1-\alpha)} \frac{1}{1-(q^2/m_V^2)} + \sum_{k=1}^N \frac{\rho_k}{1 - \frac{1}{\gamma_k} \frac{q^2}{m_V^2}}, \quad (8)$$

where α determines the strength of the dominant pole, ρ_k gives the strength of the k th term in the expansion, and $\gamma_k = m_{V_k}^2/m_V^2$, with m_{V_k} representing masses of the higher order poles. The true form factor can be approximated to any desired accuracy by introducing a large number of finely spaced effective poles. In effect, it is desirable to keep the number of terms in this expansion to a manageable number. The popular Becirevic-Kaidalov (BK) parametrization (45) is a simplified version of the $N = 1$ truncation of this expansion. In general, both the $N = 0$ case (simple pole) and the $N = 1$ case can provide good representation of the data if the pole masses are allowed to be non physical. An alternative approach (50) utilizes a series expansion around an arbitrary q^2 value t_0 . To achieve a convergent series, the expansion is formulated as an analytic continuation of the form factors in the complex $t = q^2$ plane. There is a branch cut on the real axis for $t > (M_D + M_{K,\pi})^2$, which corresponds to a region associated with production of states with appropriate quantum numbers. The convergence is accelerated by mapping the whole cut region onto the unit disk $z < 1$, where z is defined as

$$z(q^2, t_0) = \frac{\sqrt{t_+ - q^2} - \sqrt{t_+ - t_0}}{\sqrt{t_+ - q^2} + \sqrt{t_+ - t_0}}, \quad (9)$$

where $t_{\pm} = (M_D \pm M_{K,\pi})^2$ and t_0 is the arbitrary q^2 value that maps onto $z = 0$. The form factors are then expressed as (50)

$$f_+(q^2) = \frac{1}{P(q^2)\Phi(q^2, t_0)} \sum_{k=0}^{\infty} \alpha_k(t_0) [z(q^2, t_0)]^k \quad (10)$$

with $P(q^2) = z(q^2, m_V^2)$, which accounts for the pole in the form factor at $q^2 = m_V^2$. The physical observables are not expected to depend on $\Phi(q^2, t_0)$, which can be any analytical function, or t_0 .

Unquenched lattice *QCD* calculations for $D \rightarrow K\ell\bar{\nu}$ and $D \rightarrow \pi\ell\nu$ have recently been reported (12). The chiral extrapolation is performed at fixed $E = v \cdot p_{K(\pi)}$. The lattice ‘‘data points’’ are fitted to the BK parametrization (45)

$$\begin{aligned} f_+(q^2) &= \frac{f_+(0)}{(1-\tilde{q}^2)(1-\alpha\tilde{q}^2)}, \\ f_0(q^2) &= \frac{f_+(0)}{1-\tilde{q}^2/\beta}, \end{aligned} \quad (11)$$

where $\tilde{q}^2 = q^2/m_{D^*}^2$, and α and β are fit parameters. The fitted parameters are shown in Table 4. The FOCUS experiment (46) was the first to perform a non-parametric measurement of the shape of the form factor in $D \rightarrow K\mu\nu_{\mu}$ (51). CLEO-c (52), Belle (7), and BaBar (53) reported similar analyses. Fig. 3 shows the lattice *QCD* predictions for $D \rightarrow K\ell\nu$ and $D \rightarrow K\ell\nu$ with the Belle data points superimposed. Table 5 summarizes the experimental form factor fits compared to the lattice *QCD* predictions. By combining the information of the

measured leptonic and semileptonic width, a ratio independent of $|V_{cd}|$ can be evaluated, which can serve as a check of the theoretical calculations. For instance, assuming isospin symmetry, i.e. $\Gamma(D \rightarrow \pi e^+ \nu_e) = \Gamma(D^0 \rightarrow \pi^- e^+ \nu_e) = 2\Gamma(D^+ \rightarrow \pi^0 e^+ \nu_e)$, a ratio

$$R \equiv \sqrt{\Gamma(D^+ \rightarrow \mu \nu_\mu) / \Gamma(D \rightarrow \pi e^+ \nu_e)}$$

can be formed. Using the recent unquenched lattice QCD calculations (10,12), this ratio can be computed to be

$$R_{sl}^{th} = \sqrt{\frac{\Gamma^{th}(D^+ \rightarrow \mu \nu_\mu)}{\Gamma^{th}(D \rightarrow \pi e \nu_e)}} = 0.212 \pm 0.028,$$

The quoted error is evaluated through a careful study of the theory statistical and systematic uncertainties, assuming Gaussian errors. The corresponding ‘‘experimental’’ ration can be calculated using the CLEO-c f_D and isospin averaged $\Gamma(D \rightarrow \pi e^+ \nu_e)$,

$$R_{sl}^{exp} = \sqrt{\frac{\Gamma^{exp}(D^+ \rightarrow \mu \nu)}{\Gamma^{exp}(D \rightarrow \pi e \nu_e)}} = 0.249 \pm 0.022.$$

The theoretical calculations and data are consistent at 28% confidence level.

2.6 The CKM Matrix

An important goal of the next generation of precision experiments is to perform direct measurements of each individual parameter. This will enable us to perform additional unitarity checks with precision similar to that achieved currently with the first row (47). With the help of the unitarity constraints, charm-quark-related V_{cd} and V_{cs} are now determined with rather high precision (33). The most recent results from LEP II, using the $W \rightarrow \ell \nu$ branching fraction, and additional inputs from other CKM parameter measurement is $V_{cs} = 0.976 \pm 0.014$ (48). The unitarity constraint implies $V_{cd} \sim V_{us} = 0.2227 \pm 0.0017$ (47).

CLEO-c (49) has extracted $|V_{cd}|$ and $|V_{cs}|$ by combining the $|V_{cq}|f_+(0)$ results from the three parameter series expansion fit (50) with the unquenched lattice QCD predictions for $f_+(0)$ (12) to obtain

$$\begin{aligned} |V_{cs}| &= 1.015 \pm 0.010 \pm 0.011 \pm 0.106 \\ |V_{cd}| &= 0.217 \pm 0.009 \pm 0.004 \pm 0.023 \end{aligned}$$

The first two errors are experimental, statistical and systematic, while the last errors are theoretical, dominated by the discretization uncertainties in the lattice QCD charm quark action, which should be improved in the near future. It will be interesting to see a unitarity check performed on the second row of the CKM matrix element once these errors are further reduced.

2.7 Form Factors in Semileptonic $D \rightarrow V \ell \nu$ Decays

The structure of the hadronic current in semileptonic decays including vector mesons in the final state is more complex, involving four independent form factors,

V , A_0 , A_1 , and A_2 ,

$$\begin{aligned}
\langle K^*(\rho) | \bar{q} \gamma_\mu c | D \rangle &= 2 \frac{V(q^2)}{m_D + m_{K^*(\rho)}} \epsilon_{\mu\nu\alpha\beta} p_D^\nu p_{K^*(\rho)}^\alpha \epsilon^{*\beta}, \\
\langle K^*(\rho) | \bar{q} \gamma_\mu \gamma_5 c | D \rangle &= i (m_D + m_{K^*(\rho)}) \left(\epsilon_\mu^* - \frac{\epsilon^* \cdot q}{q^2} q_\mu \right) A_1(q^2) \\
&\quad - i \frac{\epsilon^* \cdot q}{m_D + m_{K^*(\rho)}} \left(P^\mu - \frac{m_D^2 - m_{K(\pi)}^2}{q^2} q^\mu \right) A_2(q^2) \\
&\quad + 2im_D \frac{\epsilon^* \cdot q}{q^2} q_\mu A_0(q^2),
\end{aligned} \tag{12}$$

where ϵ^* is a polarization of the final state meson. The vector form factor V is dominated by vector meson resonance exchanges, A_0 is dominated by pseudoscalar meson resonance exchanges, A_1 and A_2 are dominated by axial meson resonance exchanges. Generally a single pole form factor is assumed, both in experimental studies and in theoretical calculations of the normalization of the form factors. The FOCUS experiment has developed an interesting technique that extends its non-parametric determination of the form factors in $D^0 \rightarrow K^- \mu^+ \nu_\mu$ to $D^+ \rightarrow K^- \pi^+ e^+ \nu_e$ (55), later adopted also by the CLEO-c experiment (56). This method allows model independent determinations of the form factors and thus provides a better check for theoretical calculations. For example, Fajfer and Kamenic have studied these decays by including contributions of charm meson resonances beyond the simple pole (57) and have found that including two poles in the vector form factor improves the agreement between their predictions and experimental results.

The FOCUS experiment (58) has reported evidence for the presence of a small even $K^- \pi^+$ amplitude interfering with the dominant \bar{K}^{*0} component in the decay $D^+ \rightarrow K^- \pi^+ \mu^+ \nu_\mu$. CLEO-c (56) has seen the same effect in $D^+ \rightarrow K^- \pi^+ e^+ \nu_e$. This observation opens up new areas of investigation in exclusive charm semileptonic decays, namely the investigation of light quark spectroscopy. For example, it would be interesting to verify whether this broad s-wave resonance can be identified with the κ seen in D^+ Dalitz plot analyses (59). It will be interesting to search for similar interference phenomena in D_s semileptonic decays.

3 RARE AND RADIATIVE DECAYS

3.1 Theoretical Motivation

Rare charm decays hold great potential to be a sensitive probe of NP. Among all rare charm transitions, the most interesting are the decays that are associated with $\Delta C = 1$ flavor-changing neutral currents (FCNC), i.e. transitions that change charm quark quantum number by one unit while conserving the electrical charge of participating quarks. Examples of such transitions include (a) rare radiative decays mediated by $c \rightarrow u\gamma$ or $c \rightarrow u\gamma\gamma$ quark currents, or (b) rare leptonic and semileptonic decays mediated by $c \rightarrow u\ell\ell$ quark currents. Here ℓ could either be a charged lepton such as e or μ or a neutrino ν . In addition, fully non-leptonic FCNC, such as $c \rightarrow ug$ or $c \rightarrow uq\bar{q}$ are possible. We shall discuss them in Section 4.

In the SM, where FCNC cannot occur at the tree level, this is usually associated with large contribution of top quark to one-loop electroweak diagrams due to

the Glashow-Iliopoulos-Maiani (GIM) mechanism (60). This assures that the bottom-type FCNC decay is dominated by the short-distance contributions and therefore is reliably computable. It has become evident that this situation is not realized in charm decays due to relatively small mass of the bottom quark and significant hadronic dynamical effects in the region of charmed hadron mass. This leads to overwhelming long-distance contributions and decreased reliability of theoretical predictions. Indeed, model-dependent evaluations of long-distance effects are possible (61, 62), which can be used to judge relative importance of long- and short-distance physics.

These facts can constitute a problem for proper interpretation of new physics effects in FCNC processes. In addition, constraints on the strength of new interactions can be unambiguously placed only if the SM contributions are significantly smaller than the experimentally placed bound on a branching ratio.

3.1.1 INCLUSIVE AND EXCLUSIVE RADIATIVE DECAYS $c \rightarrow u\gamma$. Since rare radiative decays are two-body-decays, a branching ratio for exclusive or inclusive transitions is the primary observable. Thus, one has to evaluate relative NP/SM contribution for each model of NP. Only if the SM contribution, even dominated by the LD physics, is seen to be much smaller than current experimental bounds and possible NP contributions, such measurements can be useful in constraining NP models. Current theoretical estimates put decays rates of $D^0 \rightarrow \rho\gamma$ at the level of $(0.1 \div 0.5) \times 10^{-5}$ and $D^0 \rightarrow \phi\gamma$ at $(0.1 \div 3.4) \times 10^{-5}$. Currently, the decay $D^0 \rightarrow \phi\gamma$ has been measured to be $(2.6_{-0.61}^{+0.70+0.15}) \times 10^{-5}$ (65), and experimental constraints on other radiative decays are of the order of 10^{-4} (33). As the experimental bounds for radiative decays are pushed towards the SM theoretical estimates, these decays become less and less suitable to provide unambiguous constraints on New Physics models (62).

In the SM, the radiative charm decays occur via the operators of the type $O_7 = (e/16\pi^2)m_c(\bar{u}\sigma_{\mu\nu}P_Rc)F^{\mu\nu}$. In total, renormalization group running of perturbative QCD requires a complete set of ten operators to describe this transition (61). Note that due to the chiral structure of the SM, the contribution of a similar operator $O_7' = (e/16\pi^2)m_u(\bar{u}\sigma_{\mu\nu}P_Lc)F^{\mu\nu}$ is suppressed by a small factor m_u/m_c . Such suppression is not universal and is in fact absent in some models of NP, including SUSY. Thus, measurement of polarization of the final state photon can in principle be a nice probe of NP.

3.1.2 RARE DECAYS $D \rightarrow X_u\ell^+\ell^-$. Decays of the type $c \rightarrow u\ell^+\ell^-$ may allow a better separation of SM and NP effects. The simplest possible decay that is generated by this current is $D^0 \rightarrow \ell^+\ell^-$. Decays of this type are helicity-suppressed, with decay rates proportional to the masses squared of the final state leptons. This makes decays $D^0 \rightarrow e^+e^-$ prohibitively small. Even the decay $D^0 \rightarrow \mu^+\mu^-$ is quite small. A calculation of short distance SM effects predicts a branching fraction of about 10^{-18} (62). Long distance contributions bring the predicted branching fraction to an excess of 10^{-13} , more precisely $2.6 \times 10^{-5} \mathcal{B}(D^0 \rightarrow \gamma\gamma)$ (62). Thus, decays of this type provide almost background-free constraints on NP models. For example, R-parity-violating SUSY contributions are predicted at the level of 3×10^{-6} for some region of SUSY parameter space.

In that sense, three body decays are more suitable for experimental studies, as they do not receive the above-mentioned helicity suppression. The two modes that have been studied most extensively are $D \rightarrow \pi\ell^+\ell^-$ and $D \rightarrow \rho\ell^+\ell^-$. These more complex final states provide additional tools to disentangle SM short and

long distance effects and NP phenomena. Figure 4 from Ref. (62) illustrates this point with reference to the decay $D^+ \rightarrow \pi^+ e^+ e^-$. It shows the predicted dilepton mass distribution normalized to Γ_{D^+} . The solid line represents the total SM prediction, while the curves represent predictions from a variety of minimal supersymmetric models. It is clear that for dilepton masses close to vector meson resonances such as ρ or ϕ there is no sensitivity to new physics contributions, however there are regions where NP effects are unambiguous. In particular, the region of low $M_{e^+e^-}$ is of great interest. Similar considerations apply to $D \rightarrow \rho \ell^+ \ell^-$, where additional information is provided by the lepton forward-backward asymmetry

$$A_{FB}(q^2) \equiv \frac{\int_0^1 d\Gamma/(dq^2 dx) dx - \int_{-1}^0 d\Gamma/(dq^2 dx) dx}{d\Gamma/dq^2} \quad (13)$$

where $x = \cos \theta$. Here θ is the angle between the ℓ^+ and the D meson in the D rest frame. In the SM $A_{FB}(q^2)$ is negligibly small for all values of q^2 .

3.2 Experimental Information

A rare D radiative decay has recently been seen by Belle (65) with the reported branching ratio $\mathcal{B}(D^0 \rightarrow \phi \gamma) = (2.6_{-0.61}^{+0.70+0.15}) \times 10^{-5}$. This branching fraction is measured by studying simultaneously the decays $D^0 \rightarrow \phi \gamma$, $D^0 \rightarrow \phi \pi^0$, and $D^0 \rightarrow \phi \eta$, as the last two modes, with higher branching fractions, induce some peaking background. $D^0 \rightarrow \phi \gamma$ is dominated by long distance effects, and the branching fraction is at the level expected from theoretical estimates.

The most stringent limits on the di-lepton channels have been obtained recently by CDF (66), who study $D^0 \rightarrow \mu^+ \mu^-$ and BaBar (67) who study both $D^0 \rightarrow \mu^+ \mu^-$ and $D^0 \rightarrow e^+ e^-$. Both experiments use a D^* tagged sample and normalize their results with respect to $D^0 \rightarrow \pi^+ \pi^-$.

The channel $c \rightarrow u \ell^+ \ell^-$ has been studied by CLEO-c(64), BaBar (67), and D0 (68). The CLEO-c study focuses on $D^+ \rightarrow \pi^+ e^+ e^-$ because of their excellent sensitivity to di-electron final states, while BaBar studies both di-muon and di-electron final states of D^+ , D_s^+ and Λ_c^+ . D0 has very recently reported results on the $D^+ \rightarrow \pi^+ \mu^+ \mu^-$ final state. All three experiments start by measuring $D^+ \rightarrow \pi^+ \phi \rightarrow \ell^+ \ell^- \pi^+$ to establish the order of magnitude of long distance effects. CLEO-c finds two events with an expected background of 0.02 events, BaBar finds 19 events over a background of 40 events, and D0 finds 115 events over a background of 850 events. They find the branching fractions:

$$\begin{aligned} \mathcal{B}(D^+ \rightarrow \phi \pi^+ \rightarrow e^+ e^- \pi^+) &= (2.8 \pm 1.9 \pm 0.2) \times 10^{-6} \quad [(64)] \\ &= (2.7_{-1.8}^{+3.6}) \times 10^{-6} \quad [(67)], \end{aligned} \quad (14)$$

and

$$\mathcal{B}(D^+ \rightarrow \phi \pi^+ \rightarrow \mu^+ \mu^- \pi^+) = (1.8 \pm 0.5 \pm 0.6) \times 10^{-6} \quad [(68)]. \quad (15)$$

These experiments establish also 90 % confidence level upper limits on the short distance components of these branching fractions. Their results, compared with a representative sample of theoretical expectations based on NP scenarios are summarized in Table 6. These data show that experiments are reaching a sufficient sensitivity to limit the NP parameter space. The availability of higher statistics data samples from $e^+ e^-$ experiments and collider experiments, as LHCb, when data taking starts, bear the promise of more stringent tests in the near future.

4 HADRONIC DECAYS

Hadronic decays are interesting for several reasons. Absolute measurements of D meson branching fractions affect our knowledge of several D and B meson decays, from which CKM parameters are extracted. Multi-body final states provide information on light quark spectroscopy. Nonleptonic decays of charmed hadrons provide needed information (72) which helps in determinations of CKM angles β (73) and γ (74) in B decays and, can also help in determination of $D^0 - \bar{D}^0$ mixing parameters free from knowledge of hadronic strong phases (75).

4.1 Theoretical Considerations

Theoretical description of fully hadronic decays is significantly more complicated than leptonic or semileptonic ones, even though relevant effective Hamiltonians look quite similar to Eq. (1). Charmed nonleptonic decays are usually classified by the degree of CKM suppression. Least suppressed, where the quark level transitions are $c \rightarrow su\bar{d}$ are labeled ‘‘Cabibbo favored’’ (CF) decays and governed by

$$\begin{aligned} \mathcal{H}_{CF} &= \frac{G_F}{\sqrt{2}} V_{ud} V_{cs}^* [C_1(\mu) \mathcal{O}_1 + C_2(\mu) \mathcal{O}_2] + \text{h.c.}, \\ \mathcal{O}_1 &= (\bar{s}_i \Gamma_\mu c_i) (\bar{u}_k \Gamma^\mu d_k), \quad \mathcal{O}_2 = (\bar{s}_i \Gamma_\mu c_k) (\bar{u}_k \Gamma^\mu d_i) \end{aligned} \quad (16)$$

where $C_n(\mu)$ are the Wilson coefficients obtained by perturbative QCD running from M_W scale to the scale μ relevant for hadronic decay, and the Latin indices denote quark color.

The ‘‘Cabibbo suppressed’’ (CS) transitions are driven by $c \rightarrow du\bar{d}$ or $c \rightarrow su\bar{s}$ quark processes. Due to the presence of the quark-antiquark pair of the same flavor in the final state, the effective Hamiltonian takes much more elaborate form,

$$\begin{aligned} \mathcal{H}_{CS} &= \frac{G_F}{\sqrt{2}} \sum_{q=s,d} V_{uq} V_{cq}^* [C_1(\mu) \mathcal{O}_1^q + C_2(\mu) \mathcal{O}_2^q] \\ &\quad - \frac{G_F}{\sqrt{2}} V_{ub} V_{cb}^* \sum_{n=3}^6 C_n(\mu) \mathcal{O} + \text{h.c.}, \\ \mathcal{O}_1 &= (\bar{q}_i \Gamma_\mu c_i) (\bar{u}_k \Gamma^\mu q_k), \quad \mathcal{O}_2 = (\bar{q}_i \Gamma_\mu c_k) (\bar{u}_k \Gamma^\mu q_i), \end{aligned}$$

where $q = d, s$, and \mathcal{O}_{3-6} are the so-called ‘‘penguin’’ operators of the type $(\bar{u}c)_{V-A} \sum_q (\bar{q}q)_{V\pm A}$ (see, e.g. Ref. (76)).

The ‘‘Doubly Cabibbo suppressed’’ (DCS) decay is the one in which $c \rightarrow du\bar{s}$ quark transition drives the decay. The effective Hamiltonian for DCS decay can be obtained from Eq. (16) by interchanging $s \leftrightarrow d$.

Calculations of hadronic decay rates governed by these transitions are quite complicated and model-dependent. Most often, simplified assumptions, such as factorization (77, 78) are used to estimate the needed branching ratios. Some dynamical approaches, such as QCD sum rules, have been used to justify those assumptions (79). Charmed mesons populate the energy range where non-perturbative quark dynamics is active. This leads to resonance effects that affect the phases of nonleptonic decay amplitudes (80). Finally, standard methods of flavor $SU(3)$ can be used in studies of non-leptonic D-meson decays (81).

4.2 Branching Fraction Measurements

CLEO-c use tagged samples to obtain precise values for absolute hadronic branching fractions for D^0 and D^+ (82), and for D_s (83). Their “double-tag technique” is similar to the one developed by Mark III (84). From data at the $\psi(3770)$ they use three D^0 decay modes ($D^0 \rightarrow K^-\pi^+$, $D^0 \rightarrow K^-\pi^+\pi^0$, $D^0 \rightarrow K^-\pi^+\pi^-\pi^+$), and 6 D^+ modes ($D^+ \rightarrow K^-\pi^+\pi^+$, $D^+ \rightarrow K^-\pi^+\pi^+\pi^0$, $D^+ \rightarrow K_S\pi^+$, $D^+ \rightarrow K_S\pi^+\pi^0$, $D^+ \rightarrow K_S\pi^+\pi^-\pi^+$, $D^+ \rightarrow K^+K^-\pi^+$). Single and double tag yields are used to extract the branching fractions and $D\bar{D}$ yields from a combined fit (85) to all the measured yields. This powerful technique, combined with careful efficiency studies based on data, dominates the present world averages (33). Corrections for final state radiation are included in these branching fractions. The large numbers of $D\bar{D}$ pairs, $N_{D^0\bar{D}^0} = (1.031 \pm 0.017) \times 10^6$ and $N_{D^+D^-} = (0.819 \pm 0.012) \times 10^6$ assure measurements at the 3% level, limited by systematic uncertainties. They apply a similar technique to derive absolute D_s branching fractions from data at a center-of-mass energy of ~ 4170 MeV (83). Here the dominant final state is $D_s D_s^*$, thus the analysis is more complex because of the γ from the D_s^* .

B factories use D samples produced inclusively in B meson decays, or partially reconstructed samples of D or D_s recoiling against a fully reconstructed charmed meson as normalization. Absolute branching fraction measurements for hadronic decays of D^0 , D^+ , and D_s are summarized in Table 7, which include new absolute BF’s for $D^0 \rightarrow K^-\pi^+$, reported by BABAR (86) with approximately a 2% uncertainty, and from Belle (87) who measured the corresponding quantity for $D_s \rightarrow K^+K^-\pi^+$ with a precision of $\sim 14\%$.

In the BABAR measurement (86), $\bar{B}^0 \rightarrow D^{*+}X\ell^-\bar{\nu}_\ell$ with $D^{*+} \rightarrow D^0\pi_s^+$ are identified by partial reconstruction. Events with a lepton ℓ^- and a slow pion π_s^+ that could come from a D^{*+} are selected by studying the reconstructed ν invariant mass squared $M_{\nu,\text{meas}}^2$ inferred from conservation of energy and momentum in the center-of-mass (CMS) system, using the D^* 4-momentum inferred from π_s and the measured charged lepton’s 4-momentum. The \mathcal{B} normalization is determined from the peak in $M_{\nu,\text{meas}}^2$ (centered near 0 for real D^0 events). Backgrounds under this peak, coming from D^{**} , other $B\bar{B}$ combinations and continuum, are estimated from a wrong-sign lepton sample. Uncertainties in these backgrounds and in charged track reconstruction and particle identification efficiencies, dominate the systematic errors.

The Belle result (87) uses partially reconstructed $e^+e^- \rightarrow D_s^{*+}D_{s1}^-$ (2536) events where $D_s^{*+} \rightarrow D_s\gamma$. They study two partially reconstructed samples: in the first, the D_s is not reconstructed, but the D_{s1}^- (2536) is fully reconstructed in its decay to $\bar{D}^{*0}K^-$ and $\bar{D}^{*-}K_S$. The soft γ from the recoiling D_s^{*+} is also required. In the other normalization sample, the D_s is fully reconstructed in its $K^+K^-\pi^+$ decay mode and is combined with the γ to form a D_s^{*+} . A recoil K from the D_{s1}^- decay was also required but the D_{s1}^- (2536) was not reconstructed. The result, obtained from the ratio of the $K^+K^-\pi^+$ signal in the first mode to the D_{s1}^- signal in the second, together with the (well-known) $D^{*+} \rightarrow D^0\pi^+$ and $D_s^{*+} \rightarrow D_s\gamma$ BF’s, provided the required BF for $D_s \rightarrow K^+K^-\pi^+$.

Of special interest are the decays to K^0 . CLEO-c (88) has recently studied both the $K_L\pi$ and $K_S\pi$ final states. The K_L are identified as a peak in the missing mass. Effects of quantum correlations from the coherent D pairs from

$\psi(3770)$ decay are carefully taken into account. They measured the asymmetries

$$R(D) = \frac{\mathcal{B}(D \rightarrow K_S\pi) - \mathcal{B}(D \rightarrow K_L\pi)}{\mathcal{B}(D \rightarrow K_S\pi) + \mathcal{B}(D \rightarrow K_L\pi)}$$

for $D = D^0$ and $D = D^+$. As pointed out in Ref. (89) $D^0 \rightarrow K^0\pi^0$ involves interference between CF and DCS modes and, since we observe K^0 without knowing its strangeness, the K_S and K_L are related to give an asymmetry $R(D) = 2 \tan \theta_C$ where θ_C is the Cabibbo angle. Rosner has observed (90) that SU(3) flavor symmetry, specifically U -spin symmetry, predicts that the ratio of amplitudes for $D^0 \rightarrow K^0\pi^0$ to $D^0 \rightarrow \bar{K}^0\pi^0$ is $\tan^2 \theta_C \sim 0.054$. This leads to the prediction that the value for $D(D^0)$ should be $2 \tan^2 \theta_C \sim 0.109 \pm 0.001$. Ref. (88) finds $D(D^0) = 0.108 \pm 0.025 \pm 0.024$, significantly different from zero, and in good agreement with this prediction. There are no predictions for $R(D^+)$, measured to be $0.022 \pm 0.016 \pm 0.018$, compatible with zero.

4.2.1 CABIBBO SUPPRESSED HADRONIC DECAYS. Due to CKM suppression, these rates are expected to be lower by a factor $r_{cs} = |(V_{cs}V_{us}) / (|V_{cs}V_{ud})|^2 \approx 0.05$ relative to CF rates.

Using their $281 \text{ pb}^{-1} \psi(3770)$ sample, CLEO-c (91) measured branching fractions for many multi-pion, η and ω decay modes of D^0 and D^+ mesons. They use single tags and they extract absolute branching fractions using the corresponding well measured CF modes for normalization. These branching fractions range from $(1 - 4) \times 10^{-3}$ and are measured with a precision of about (5 - 10)%. The largest rates are $D^0 \rightarrow \pi^-\pi^+\pi^0$ ($13.2 \pm 0.6 \times 10^{-3}$) for D^0 and $D^+ \rightarrow \pi^-\pi^+\pi^+$ ($3.35 \pm 0.22 \times 10^{-3}$) and $D^+ \rightarrow \eta\pi^+$ ($3.61 \pm 0.36 \times 10^{-3}$) for D^+ . These measurements represent a significant improvement on previous knowledge, frequently being first observations. The results are generally consistent with simple CKM suppression. However, only an upper limit is extracted for $D^0 \rightarrow 3\pi^0$, in spite of the large \mathcal{B} observed for $D^0 \rightarrow \pi^-\pi^+\pi^0$. A possible explanation is that the 3 pions are produced predominantly in an $I = 0$ state, inaccessible to this mode, after a $\Delta I = 1/2$ transition.

The di-pion modes, $D^+ \rightarrow \pi^+\pi^0$, $D^0 \rightarrow \pi^+\pi^-$ and $D^0 \rightarrow \pi^0\pi^0$ are related by two amplitudes A_0 and A_2 corresponding, respectively, to the S -wave di-pion isospin $I = 0$ and $I = 2$ states produced

$$\begin{aligned} A^{+0} &= \sqrt{\frac{3}{2}}A_2 & A^{+-} &= \sqrt{\frac{2}{3}}A_0 + \sqrt{\frac{1}{3}}A_2 \\ A^{00} &= \sqrt{\frac{1}{3}}A_0 - \sqrt{\frac{2}{3}}A_2 \end{aligned} \quad (17)$$

Following the procedure outlined in Ref. (92), CLEO obtains (91) from these new results $|A_2/A_0| = 0.420 \pm 0.014 \pm 0.01$ and $\arg(A_2/A_0) = (86.4 \pm 2.8 \pm 3.3)^\circ$, which is rather large.

A long standing puzzle is found in the ratio $\mathcal{R}(D^0 \rightarrow K^+K^-)/\mathcal{R}(D^0 \rightarrow \pi^+\pi^-) = 3.53 \pm 0.12$ where \mathcal{R} are BF's corrected for the 2-body phase space factor.

BABAR (93) has measured the branching fractions

$$\begin{aligned} \mathcal{B}(D^0 \rightarrow \pi^+\pi^-\pi^0) &= (1.493 \pm 0.008 \pm 0.055) \times 10^{-2} \\ \mathcal{B}(D^0 \rightarrow K^+K^-\pi^0) &= (0.334 \pm 0.004 \pm 0.015) \times 10^{-2}. \end{aligned}$$

The corresponding ratio for decays where an extra π^0 is produced gives $\mathcal{M}(D^0 \rightarrow K^+K^-\pi^0)/\mathcal{M}(D^0 \rightarrow \pi^+\pi^-\pi^0) = 0.678 \pm 0.027$, in clear contrast to the 2-body ratio above. This result has recently been confirmed by Belle (94).

CLEO-c also studied $D_s \rightarrow PP$ modes (95), where “ P ” is any pseudo-scalar meson, using their $\sqrt{s} = 4170$ MeV sample. The modes ($K^+\eta$, $K^+\eta'$, π^+K_S , $K^+\pi^0$) are seen for the first time and are compared with their CF counterparts $\pi^+\eta$, $\pi^+\eta'$ and K^+K_S . The ratios observed are reasonably consistent with the value of $r_{\text{CS}} \approx 5\%$. The decays $D_s \rightarrow \pi^+\pi^0$ have not yet been seen. The di-pions would be in an S -wave with $I = 2$, and would have to be reached through a $\Delta I = 2$ transition, apparently much suppressed.

4.2.2 DOUBLE CABIBBO SUPPRESSED HADRONIC DECAYS ($c \rightarrow du\bar{s}$) OF D MESONS. These decays are expected to be suppressed relative to CF modes by a factor $r_{\text{DCS}} = |(V_{cd}V_{us}) / (|V_{cs}V_{ud})|^2 \approx 3.1 \times 10^{-3}$. For D^0 's, these rates are comparable to the mixing rate so that the two processes interfere; therefore disentangling the two effects needs some care. This is discussed in more detail in Section 5.

With such small branching ratios, one might wonder if DCS transitions could be affected by NP effects. However, since the final state is composed of quarks of different flavors, it is hard to find a well-motivated NP model that can affect DCS transition at an appreciable level (96).

The D^0 DCS branching fractions measured can be related, using world averages (33), to the expectations based on the value of r_{DCS}

$$\begin{array}{lll} (K^+\pi^-) & (1.45 \pm 0.04) \times 10^{-4} & (1.18 \pm 0.26) \times r_{\text{DCS}} \\ (K^+\pi^-\pi^0) & (2.96 \pm 0.19) \times 10^{-4} & (2.50 \pm 0.57) \times r_{\text{DCS}} \\ (K^+\pi^-) & (2.49_{-0.19}^{+0.21}) \times 10^{-4} & (2.10 \pm 0.49) \times r_{\text{DCS}}. \end{array}$$

The only decay of D^+ , free from mixing effects, so far observed is $D^+ \rightarrow K^+\pi^0$. BABAR (97) obtain $\mathcal{B} = (2.52 \pm 0.47 \pm 0.25 \pm 0.08) \times 10^{-4}$ and CLEO-c (98) obtain $\mathcal{B} = (2.28 \pm 0.36 \pm 0.15 \pm 0.08) \times 10^{-4}$. Both experiments use the $D^+ \rightarrow K^-\pi^+\pi^+$ as normalization, and the fourth uncertainty in each case is due to this.

The decay of $D^+ \rightarrow K^+\pi^0$ has been observed by BABAR and confirmed with a more precise measurement by CLEO-c. Combining these measurements with the known lifetimes for D^0 and D^+ and the $D^0 \rightarrow K^-\pi^+$ BF's from ref. (33), a ratio can be formed,

$$\frac{\Gamma(D^+ \rightarrow K^+\pi^0)}{\Gamma(D^0 \rightarrow K^-\pi^+)} = (2.44 \pm 0.33) \times 10^{-3} = (0.79 \pm 0.20) \times r_{\text{DCS}}$$

which is clearly compatible with the expected DCS rate. Similarly, the ratio of the two DCS rates is

$$\frac{\Gamma(D^+ \rightarrow K^+\pi^0)}{\Gamma(D^0 \rightarrow K^+\pi^-)} = 0.66 \pm 0.09.$$

A naive spectator diagram analysis would predict a ratio of 0.5. The difference is probably due to final state interaction effects, although annihilation or exchange diagrams could also contribute.

4.3 Three Body Decays

Multi-body D meson decays are a very rich source of information on long range strong interaction effects because of the complex interference patterns between

intermediate resonances formed between hadrons in the final states. In addition, some of them are relevant for CPV measurements in B decays (74) or $D^0 - \bar{D}^0$ mixing parameters (73). A vast body of experimental data has been studied, from fixed target experiments, CLEO (from data sets both near the $\Upsilon(4S)$ and at 3770 MeV center-of-mass energies), BABAR and Belle. Huge data samples - of order 10^6 events in many channels - from the B factories have led to the need to review models used to fit the Dalitz plot distributions. Many results, no doubt, await such review and are yet to be published. Of particular concern is the extent to which phase information, essential to the determination of the parameters above, depends on the models assumed for these fits. Efforts are underway to attempt less model-dependent approaches (99, 100).

4.3.1 FORMALISM FOR THREE-BODY D AND D_s DECAYS Decays of D or D_s to three hadrons ABC often proceed through quasi 2-body modes $D \rightarrow A + f$ followed by $f \rightarrow B + C$, where f is an intermediate ‘‘isobar’’ state, as outlined in Ref. (77). When A , B and C are pseudo-scalar hadrons, the Dalitz plot, in which the squared invariant mass of one hadron pair is plotted against the squared invariant mass of one of the other pairs, contains all the dynamical information. These Dalitz plots often show intricate interference patterns between multiple resonances that may be produced in an intermediate state.

The decay amplitude could be constructed from a partial wave expansion in any one of the three possible channels f defined by the particle pair. Here we choose $f = BC$. Each wave would then be characterized by the spin ($J = L$ for pseudo-scalar hadrons) and isospin I of f

$$\mathcal{A}(s, s') = \sum_I \sum_{L=0}^{\infty} M_L(p, q) F_{L,I}(s) \quad (18)$$

where s and s' are squared invariant masses for BC (i.e. f) and for the AC channel, respectively. $F_{L,I}$ is the partial wave decay amplitude for the system f . M is a tensor function appropriate for the conservation of total spin in the decay and depends on L and the momenta p and q of B and A , respectively, that are defined in the f rest frame. The density of points on the Dalitz plot is then proportional to $|\mathcal{A}|^2$.

The complex function $F_{L,I}(s)$ describes the production and final state scattering resulting in the observed system f . Two distance scales may be distinguished. In the first, the parent D decays weakly, and hadronization occurs making an intermediate hadron state k that may differ from f . At longer range, re-scattering (e.g. $KK \rightarrow \pi\pi$) occurs to make the observed system f . Thus, dropping label L and I , $F_{L,I}(s)$ can be written

$$F_f(s) = T_{fk}(s) Q_k(s) \quad (19)$$

in which $T_{fk}(s)$ is the matrix that describes hadron-hadron scattering. When s is small, T can only include elastic scattering. In this regime, therefore, *in the absence of scattering between k and the recoil hadron A* , the Watson theorem (101) requiring that the phase of $F_f(s)$ should have the same s -dependence as elastic scattering, should hold. However, $Q_k(s)$ is an unknown function describing the short-range effects and could well have an s -dependent phase when strong $k-f$ scattering takes place. In this case, the Watson theorem would not hold. A recent K -matrix fit to the $I = 1/2$ $K^- \pi^+$ S -wave amplitude from $D^+ \rightarrow K^- \pi^+ \pi^+$ data by the FOCUS collaboration (102) indicate that this may be so.

4.3.2 ANALYSIS METHODS OF THREE-BODY D AND D_s DECAYS In fitting Dalitz plots, analysts have used several assumptions for the form of $F_f(s)$. Most often used so far is the Breit-Wigner “isobar model” in which $F(s)$ is approximated as a linear combination of resonant terms for each wave. Eq. (18) is approximated by a finite sum that includes only terms for the resonant states r observed in the data, *no matter in which channel they occur*. The amplitude (18) is then a sum of Breit-Wigner propagators

$$\begin{aligned} \mathcal{A}(s, s') &= NR + \sum_r A_r \\ A_r &= c_r e^{i\delta_r} \frac{M_L(p, q) G_L(q) G_L(p)}{m_r^2 - s + im_r \Gamma(s, L)} \end{aligned} \quad (20)$$

with complex coefficients $c_r e^{i\delta_r}$ and a constant term NR , often introduced to describe direct, non-resonant decay to the three hadrons A, B and C . The parent D and the resonance have form-factors G_L that depend on L . Here, m_r is the mass, and $\Gamma(s, L) = \Gamma_r(m_r/\sqrt{s})(p/p_r)^{2L+1}[G_L(p)/G_L(p_r)]^2$ is the mass-dependent width of the resonance r . The form-factors $G_L(q)$ and $G_L(p)$ for, respectively, the parent and the resonance r , are usually assumed to take the Blatt-Weisskopf form (103). Fractions are defined, for each resonance r , as

$$f_r = \frac{\int \int |A_r|^2 ds ds'}{\int \int |NR + \sum_r A_r|^2 ds ds'}. \quad (21)$$

The sum of fractions, so defined, is not required to be unity, since the interference terms, included in the denominator, are missing from the numerator. Though Eq. (21) is in standard use, a better definition would be desirable. In particular, it works only to define resonant fractions from the isobar model.

Other models attempt to address the problems associated with the description of the S -waves where the identity of resonances is less well understood. Understandably, these methods do not have a convenient definition for resonance fractions. One model introduces hadron scattering through a K -matrix (104,105). related to the K and T -matrices and Q - and F -vectors discussed above by

$$\begin{aligned} T_{kf}(s) &= (I - i\rho K(s))_{ki}^{-1} K_{if}(s) \\ Q_f(s) &= K_{fk}^{-1}(s) P_k(s) \\ F_f(s) &= (I - i\rho K(s))_{fk}^{-1} P_k(s) \end{aligned} \quad (22)$$

where ρ is a matrix of phase space factors, purely imaginary below threshold, for any of the channels included. This is real, guaranteeing the unitarity of T , and it contains poles and non-resonant terms obtained from global fits to available scattering data. For example, Anisovich and Sarantsev (106) derived a K -matrix representation of scalar $\pi\pi$ resonances through a global fit of all the available scattering data from threshold to 1900 MeV. The fit to the Dalitz plot then finds parameters for the production vector, $P_k(s)$, which is, in essence, a function that describes the dependence of production of f on s . Pros and cons are known for this model. Unlike the isobar model, whose description of broad resonances by Breit-Wigner is flawed, this does preserve the unitarity of the T -matrix. It does not, however, do this for F , since the P -vector is arbitrary. Analyticity of T is not guaranteed either, so its ability to describe poles is limited.

Less model-dependent methods are also used. In restricted regions of the Dalitz plot, the angular “moments” of f can be used to measure the S , P , etc. amplitudes. A method that works over the whole Dalitz plot was introduced by the E791 collaboration (107) in the analysis of $D^+ \rightarrow K^- \pi^+ \pi^+$ decays. $F(s)$ for the $K^- \pi^+$ S -wave was parameterized by a set of complex quantities at discrete s values. These quantities were treated as free parameters in their fit. The method requires a reference phase that, in their fit, was defined by the isobar model description of the other waves. This introduced some model-dependence in their result.

Assumptions about the models used to describe Dalitz plots affects results for CKM phases and $D^0 - \bar{D}^0$ mixing parameters. Extending such model-independence into fits becomes more important, therefore, as statistical precision of such measurements improves.

4.3.3 SUMMARY OF CHARM DALITZ PLOT ANALYSES Several experiments have analyzed $D^0 \rightarrow K_S \pi^+ \pi^-$ (33). CLEO(108) was first and included 10 resonances in their fit: $K_S \rho^0$, $K_S \omega$, $K_S f_0(980)$, $K_S f_2(1270)$, $K_S f_2(1270)$, $K_S h_0(1370)$, $K^*(892)\pi^+$, $K_0^*(1430)^- \pi^-$, $K_2^*(1430)^- \pi^+$, $K^*(1680)\pi^+$, and the doubly Cabibbo suppressed mode $K^*(892)^+ \pi^-$. CLEO found a much smaller non-resonant contribution than did the earlier experiments. The source of these contributions has been attributed to broad resonances such as the $K_0^*(1430)$. The residual small non-resonant component may be a signature of broad scalar resonances such as the κ and σ . More recently, to extract information on the CKM angle $\gamma(\phi_3)$, analyses have also been made by both Belle (109, 110) and BABAR(111) using samples two orders of magnitude larger. At this level of statistical precision, the inadequacy of a simple isobar model to describe the data is revealed. After amplitudes for a clear signal for $\rho - \omega$ mixing and for radial excitations for the ρ are added, the fit is poor. Addition of a second, probably unphysical, σ isobar, at ~ 1000 MeV/ c^2 improves the fit yet, even then, a reasonable fit quality is barely achieved. Alternate isobar models lead to uncertainties of about 10° in $\gamma(\phi_3)$, but these are smaller than the statistical and other systematic uncertainties of about 20° currently obtainable.

Decays to $D^0 \rightarrow \pi^+ \pi^- \pi^0$ are also used by BABAR to measure γ (112). The Dalitz plot, also fitted earlier by CLEO (113), is found to have a negligibly small NR component, and to be dominated by $\rho\pi$ in all three charge modes. The structure of the plot shows strong, destructive interference between these modes in a six-fold symmetry suggestive of a dominant $I = 0$. This is consistent with the observation, noted in section 4.2.1, that $D^0 \rightarrow 3\pi^0$ decays are strongly suppressed.

The decay $D^+ \rightarrow \pi^+ \pi^+ \pi^-$ was studied by E687, E791(114), FOCUS and, more recently, CLEO (115). This new CLEO analysis uses the largest sample ($\sim 4,000$ events) so far. An earlier isobar model analysis by E791 had reported the need to add a $\sigma(500)$ Breit-Wigner to the $\pi^+ \pi^-$ S -wave in order to get an acceptable fit. FOCUS re-examined this decay using a K -matrix model for the $\pi^+ \pi^-$ S -wave, including hadron scattering data from a number of earlier experiments. The fit was acceptable, but the question of whether or not there was a $\sigma(500)$ was not clear. CLEO tried various other parameterizations for $\sigma(500)$. Following a suggestion by J.Oller (116) a simple pole of the form $1/(m_0^2 - s)$ where $m_0^2 = (0.47 - 0.22i)$ was used rather than the Breit-Wigner used by E791. A scalar term based on the linear sigma model (117) was also used. Both these

approaches produced a slightly improved fit. This all suggests that a low mass σ resonance is likely to play a role in this mode, but even larger data samples are needed to find its pole parameters.

E791 found evidence for a broad $K\pi$ scalar resonance in $D^+ \rightarrow K^+\pi^+\pi^+$ (118). Their original fit needed to include a non-resonant component with a fit fraction in excess of 90%. The inclusion of an S-wave $\bar{K}\pi$ resonance with mass $797 \pm 19 \pm 43$ MeV and width $410 \pm 19 \pm 43$ MeV improved the fit considerably and reduced the non-resonant fit fraction to $13 \pm 5.8 \pm 4.4$ %. A new fit to this channel by Focus using three times the sample size and a K -matrix obtained from $K\pi$ scattering data indicates that an $I = 3/2$ $K\pi$ component is probably also present, but is unable to address the existence of a κ .

The charged S -wave $K^\pm\pi^0$ systems could provide new information on the $\kappa(800)$ seen, so far, only in the neutral $K^-\pi^+$ system. If it is an $I = 1/2$ scalar resonance, it could also appear, with similar mass and width, in charged $K\pi$ systems like this. This was a motivation for BaBar to study the decays $D^0 \rightarrow K^+K^-\pi^0$ (119). An isobar model fit is able to provide a satisfactory, though ambiguous, description of the data. In each model tried, the $K^{*+}(890)$ resonance is included among the components and is used as the reference for other phases. An S -wave K^+K^- resonance is required to obtain a satisfactory fit, but there is no distinction between $a_0(980)$ and $f_0(980)$ at low masses. The higher mass K^+K^- system also requires some contribution, and either $f'_2(1525)$ or an f_0 with a similar mass works well.

Three models are compared for the $K\pi$ S -waves. The first is a linear combination of Breit-Wigner terms for $\kappa(800)$, $K^*(1430)$ and an NR term. The κ^\pm mass and width are allowed to vary. Second is the model that describes the data from the LASS $K\pi$ scattering experiment (120). The third uses the results for this wave from the E791 model-independent $D^+ \rightarrow K^-\pi^+\pi^+$ analysis (107). The second model gives the best fit, with the LASS phases shifted by $\sim -90^\circ$. The fit with κ^\pm is poor and requires a mass (870 ± 30) MeV/ c^2 and width (150 ± 20) MeV/ c^2 , the latter differing considerably from the width of ~ 400 MeV/ c^2 reported for the neutral state. Establishing the existence of a κ state with such a width requires more sophisticated analysis to find its pole in the T matrix so, though poor, this result does not rule it out as a genuine resonance.

As the ϕ band is relatively far from other interfering vector resonances, a study of the angular moments in the region around it is undertaken in order to attempt to learn more about the underlying S -wave. The K^+K^- invariant mass distributions are plotted, weighting each event by factors $\sqrt{2\ell + \pi/4}P_\ell(\theta)$ (for $\ell = 0, 1$ and 2), where θ is the angle between the K^- and the π^0 in the K^+K^- rest frame, and P_ℓ is the Legendre polynomial function of order ℓ . These distributions, corrected for efficiency and with background subtracted, are defined as the ‘‘moments’’ X_ℓ in each mass bin. Assuming that only S - and P -waves ($L = 0$ and 1) contribute to the K^+K^- system, these moments are used to extract them:

$$X_0 = \frac{|S|^2 + |P|^2}{\sqrt{2}} ; X_1 = \sqrt{2}|S||P| \cos \theta_{SP} ; X_2 = \sqrt{\frac{2}{5}}|P|^2 \quad (23)$$

for each mass. In Fig. 5, the resulting magnitudes $|S|$ and $|P|$, corrected for the phase space in the Dalitz plot (length of the K^+K^- mass strips) are plotted. $|P|$, shown in (b), follows the ϕ line shape well, with no asymmetry and little background, up to about 1040 MeV/ c^2 .

In Fig. 5(a), $|S|$ values, determined from this channel, are compared with similar measurements of $|S|$ from an earlier analysis (114) of $D^0 \rightarrow K^+K^-K_S$ decays. In that system, $a_0^+(980)$ in the K^+K_S system was compared with the S -wave in the K^+K^- system and found to agree well, suggesting that $a_0(980)$, as opposed to $f_0(980)$ was present in both charge states. It is possible that the excellent agreement seen here is also evidence that $a_0(980)$ is the main contributor to the K^-K^+ S -wave in this decay too. A more convincing test would, however, be to analyze the $D^0 \rightarrow K^-\pi^+\eta$ and $D^0 \rightarrow \eta\pi^0K_S$ systems since the a_0 would then be more obvious in its $\eta\pi^+$ decay modes.

The last topic that we discuss is the Dalitz plot analysis of the decay $D_s \rightarrow K^+K^-\pi^+$. E687 (121) reported the first Dalitz plot analysis of this channel with a sample of ~ 300 events. They found significant scalar contributions from $f_0(980)$ (or $a_0(980)$). CLEO studied the K^+K^- invariant mass spectrum in this decay (83) and found a clear peak at the ϕ mass, but also a broad component with kinematic properties indicative of a scalar. This component is rather important because the mode $D_s \rightarrow \phi\pi$ has been commonly used for D_s decay normalization, and the presence of this scalar component introduces an additional uncertainty in this branching fraction as the scalar channel that is absorbed in the $\phi\pi$ signal depends upon the experimental cuts used. For example, CLEO found that an uncertainty of the order of 5% was introduced depending upon the cut choices. BABAR (122) recently reported a preliminary fit of the Dalitz plot structure of this decay with over 100,000 events. They studied moments in the low mass K^+K^- and $K^-\pi^+$ systems which showed clear evidence for an S -wave contribution in the former, but none in the latter. An isobar model fit shows, indeed, a strong $f_0(980)$ component, thus confirming that the $D_s \rightarrow \phi\pi$ branching fraction is not a very wise choice of normalization channel.

A lot of work is still ongoing on the experimental side, with further exploration of modes relevant for CPV studies, both in D and B decays, and on the theory side to identify tools that reduce the model dependence in the Dalitz plot analyses, in particular when broad scalar resonances are involved. The rich structure of the Dalitz plots is not only a unique and powerful asset in understanding heavy flavor decay dynamics but also a tool for disentangling the intricacies of non-perturbative strong interaction effects.

5 CHARM MIXING AND CP -VIOLATION

The phenomena of mixing and CPV in the charm sector were first discussed three decades ago (123) but the smallness of these effects are such that experimental evidence is scarce. CPV has not yet been observed, with upper limits currently at about the 1% level. On the other hand, after years of experimental investigation (33), evidence for mixing has finally been seen in two kinds of time-dependent measurements. The BABAR collaboration (124) has reported a 3.9 standard deviation effect in “wrong-sign” (WS) decays of $D^0 \rightarrow K^+\pi^-$ ¹. The CDF collaboration has reported a 3.8 standard deviation effect (147). Also, the Belle collaboration (145) has reported a 3.2 standard deviation effect arising from the observed difference in lifetimes for decays to CP even final states $D^0 \rightarrow K^+K^-$ and $\pi^+\pi^-$ compared to the mixed CP state $K^-\pi^+$. This has also been confirmed by the BABAR experiment (148). In addition, useful information on the strong

¹Unless otherwise noted, charge conjugate states are assumed throughout this paper.

phase δ affecting $D^0 \rightarrow K^+\pi^-$ mixing results is coming from CLEO-c studies that exploit the quantum coherence of the $D^0\bar{D}^0$ pair produced near threshold (33).

5.1 Charm mixing predictions in the Standard Model

The mixing arises from $|\Delta C| = 2$ interactions that generate off-diagonal terms in the mass matrix for D^0 and \bar{D}^0 mesons. The expansion of the off-diagonal terms in the neutral D mass matrix to second order in the weak interaction is

$$\left(M - \frac{i}{2}\Gamma\right)_{21} = \frac{1}{2M_D} \langle \bar{D}^0 | H_w^{|\Delta C|=2} | D^0 \rangle + \frac{1}{2M_D} \sum_n \frac{\langle \bar{D}^0 | H_w^{|\Delta C|=1} | n \rangle \langle n | H_w^{|\Delta C|=1} | D^0 \rangle}{M_D - E_n + i\epsilon}, \quad (24)$$

where $H_w^{|\Delta C|=2}$ and $H_w^{|\Delta C|=1}$ are the effective $|\Delta C| = 2$ and $|\Delta C| = 1$ Hamiltonians. The off-diagonal mass-matrix terms induce mass eigenstates D_1 and D_2 that are superpositions of the flavor eigenstates D^0 and \bar{D}^0 ,

$$D_{1,2} = p D^0 \pm q \bar{D}^0, \quad (25)$$

where $|p|^2 + |q|^2 = 1$. The key quantities in D^0 mixing are the mass and width differences,

$$\Delta M_D \equiv M_1 - M_2 \quad \text{and} \quad \Delta \Gamma_D \equiv \Gamma_1 - \Gamma_2, \quad (26)$$

or equivalently their dimensionless equivalents,

$$x_D \equiv \frac{\Delta M_D}{\Gamma_D}, \quad \text{and} \quad y_D \equiv \frac{\Delta \Gamma_D}{2\Gamma_D}, \quad (27)$$

where Γ_D is the average width of the two neutral D meson mass eigenstates. Two quantities, y_D^{CP} and y'_D , which are actually measured in most experimental determinations of $\Delta \Gamma_D$, are defined as

$$\begin{aligned} y_D^{\text{CP}} &\equiv (\Gamma_+ - \Gamma_-)/(\Gamma_+ + \Gamma_-) = y_D \cos \phi - x_D \sin \phi \left(\frac{A_m}{2} - A_{\text{prod}} \right), \\ x' &= x_D \cos \delta_{K\pi} + y_D \sin \delta_{K\pi}, \\ y' &= y_D \cos \delta_{K\pi} - x_D \sin \delta_{K\pi}, \end{aligned} \quad (28)$$

where the transition rates Γ_{\pm} pertain to decay into final states of definite CP , $A_{\text{prod}} = (N_{D^0} - N_{\bar{D}^0}) / (N_{D^0} + N_{\bar{D}^0})$ is the so-called production asymmetry of D^0 and \bar{D}^0 (giving the relative weight of D^0 and \bar{D}^0 in the sample) and $\delta_{K\pi}$ is the strong phase difference between the Cabibbo favored and double Cabibbo suppressed amplitudes (80). The quantities A_m and ϕ account for the presence of CPV in D^0 - \bar{D}^0 mixing, with A_m being related to the q, p parameters of Eq. (25) as $A_m \equiv |q/p|^2 - 1$ and ϕ a CP -violating phase of M_{21} (if one neglects direct CPV) (125).

The charm quark system is rather unique from the theoretical point of view, as its mass places it somewhere on the border of heavy and light quark systems. This makes prediction of $D^0 - \bar{D}^0$ -mixing parameters a challenging task. As was shown in (126), in the SM, x_D and y_D are generated only at second order in $SU(3)_F$ breaking,

$$x_D, y_D \sim \sin^2 \theta_C \times [SU(3) \text{ breaking}]^2, \quad (29)$$

where θ_C is the Cabibbo angle. Therefore, predicting the SM values of x_D and y_D depends crucially on estimating the size of $SU(3)_F$ breaking.

Theoretical predictions of x_D and y_D within the SM span several orders of magnitude. Roughly, there are two approaches, neither of which give very reliable results because m_c is in some sense intermediate between heavy and light. The “inclusive” approach is based on the operator product expansion (OPE). In the $m_c \gg \Lambda$ limit, where Λ is a scale characteristic of the strong interactions, ΔM and $\Delta\Gamma$ can be expanded in terms of matrix elements of local operators (127, 128, 129, 130, 131). Such calculations typically yield $x_D, y_D < 10^{-3}$. The use of the OPE relies on local quark-hadron duality, and on Λ/m_c being small enough to allow a truncation of the series after the first few terms. The charm mass may not be large enough for these to be good approximations, especially for nonleptonic D decays. An observation of y_D of order 10^{-2} could be ascribed to a breakdown of the OPE or of duality, but such a large value of y_D is certainly not a generic prediction of OPE analyses. The “exclusive” approach sums over intermediate hadronic states, which may be modeled or fitted to experimental data (132, 133, 134). Since there are cancellations between states within a given $SU(3)$ multiplet, one needs to know the contribution of each state with high precision. However, the D meson is not light enough that its decays are dominated by a few final states. In absence of sufficiently precise data on many decay rates and on strong phases, one is forced to use some assumptions. It was shown that phase space effects alone provide enough $SU(3)_F$ violation to induce $x_D, y_D \sim 10^{-2}$ (126, 135). Large effects in y_D appear for decays close to D threshold, where an analytic expansion in $SU(3)_F$ violation is no longer possible; in addition, a dispersion relation can be used to show that in this case x_D would receive contributions of similar order of magnitude.

5.2 New Physics contribution to $D^0 - \bar{D}^0$ mixing

In order to see how NP might affect the mixing amplitude, it is instructive to consider off-diagonal terms in the neutral D mass matrix of Eq. (24).

5.2.1 NP IN $|\Delta C| = 2$ INTERACTIONS. Since all new physics particles are much heavier than the SM ones, the most natural place for NP to affect mixing amplitudes is in the $|\Delta C| = 2$ piece, which corresponds to a local interaction at the charm quark mass scale. Integrating out NP degrees of freedom at some scale Λ , we are left with an effective Hamiltonian written in the form of series of operators of increasing dimension (136). The complete basis of those effective operators, which most conveniently can be done in terms of left- and right-handed quark fields, is composed of eight operators,

$$\mathcal{H}_{NP}^{\Delta C=2} = \sum_{i=1} C_i(\mu) Q_i(\mu), \quad (30)$$

where C_i are the Wilson coefficients, and Q_i are the effective operators,

$$\begin{aligned} Q_1 &= \bar{u}_L \gamma_\mu c_L \bar{u}_L \gamma^\mu c_L, & Q_5 &= \bar{u}_R \sigma_{\mu\nu} c_L \bar{u}_R \sigma^{\mu\nu} c_L \\ Q_2 &= \bar{u}_R \gamma_\mu c_R \bar{u}_L \gamma^\mu c_L, & Q_6 &= \bar{u}_R \gamma_\mu c_R \bar{u}_R \gamma^\mu c_R, \\ Q_3 &= \bar{u}_L c_R \bar{u}_R c_L, & Q_7 &= \bar{u}_L c_R \bar{u}_L c_R, \\ Q_4 &= \bar{u}_R c_L \bar{u}_R c_L, & Q_8 &= \bar{u}_L \sigma_{\mu\nu} c_R \bar{u}_L \sigma^{\mu\nu} c_R, \end{aligned} \quad (31)$$

Since these operators are generated at the scale $\mu = \Lambda$ (at which NP is integrated out), a non-trivial operator mixing can occur if we take into account renormalization group running of these operators between $\mu = \Lambda$ and $\mu \simeq m_c$ scales. This running can be accounted for by solving RG equations obeyed by the Wilson coefficient functions,

$$\frac{d}{d \log \mu} \vec{C}(\mu) = \hat{\gamma}^T(\mu) \vec{C}(\mu), \quad (32)$$

where $\hat{\gamma}^T(\mu)$ represents the matrix of anomalous dimensions of operators of Eq. (31) (136). A prediction for a mixing parameter x in a particular model of NP is then obtained by computing $C_i(\Lambda)$ for a set of $\mathcal{Q}_i(\Lambda)$ generated by a given model, running the RG equations of Eq. (32) and computing matrix elements $\langle \bar{D}^0 | \mathcal{Q}_i(m_c) | D^0 \rangle$.

Depending on the NP model, predictions for x_D vary by orders of magnitude. It is interesting to note that some models *require* large signals in the charm system if mixing and FCNCs in the strange and beauty systems are to be small (e.g. the SUSY alignment model). A list of constraints on NP models is given in Table 8 (for more informative figures and methodology please see Ref. (136)).

5.2.2 NP IN $|\Delta C| = 1$ INTERACTIONS. The local $|\Delta C| = 2$ interaction cannot, however, affect $\Delta\Gamma_D$ because it does not have an absorptive part. Thus, naively, NP cannot affect lifetime difference y . This is, however, not quite correct. Consider a D^0 decay amplitude which includes a small NP contribution, $A[D^0 \rightarrow n] = A_n^{(\text{SM})} + A_n^{(\text{NP})}$. Here, $A_n^{(\text{NP})}$ is assumed to be smaller than the current experimental uncertainties on those decay rates. Then it is a good approximation to write y as

$$y_D \simeq \sum_n \frac{\rho_n}{\Gamma_D} A_n^{(\text{SM})} \bar{A}_n^{(\text{SM})} + 2 \sum_n \frac{\rho_n}{\Gamma_D} A_n^{(\text{NP})} \bar{A}_n^{(\text{SM})} . \quad (33)$$

The SM contribution to y is known to vanish in the limit of exact flavor $SU(3)$. Moreover, the first order correction is also absent, so the SM contribution arises only as a *second* order effect. Thus, those NP contributions which do not vanish in the flavor $SU(3)$ limit must determine the lifetime difference there, even if their contributions are tiny in the individual decay amplitudes (137). A simple calculation reveals that NP contribution to y can be as large as several percent in R-parity-violating SUSY models or as small as 10^{-10} in the models with interactions mediated by charged Higgs particles (137, 138).

5.3 CP-violation

An observation of CPV in the current round of charm experiments is arguably one of the cleanest signals of physics beyond the SM (BSM).

It can be easily seen why manifestation of NP interactions in the charm system is associated with the observation of (large) CPV . This is due to the fact that all quarks that build up the hadronic states in weak decays of charm mesons belong to the first two generations. Since 2×2 Cabibbo quark mixing matrix is real, no CPV is possible in the dominant tree-level diagrams which describe the decay amplitudes. CP -violating amplitudes can be introduced in the SM by including penguin or box operators induced by virtual b -quarks. However, their contributions are strongly suppressed by the small combination of CKM matrix elements $V_{cb}V_{ub}^*$. It is thus widely believed that the observation of (large) CPV in

charm decays or mixing would be an unambiguous sign for NP. This fact makes charm decays a valuable tool in searching for NP, since the statistics available in charm physics experiment is usually quite large.

As with other flavor physics, CP -violating contributions in charm can be generally classified by three different categories:

- (I) CP violation in the $\Delta C = 1$ decay amplitudes. This type of CPV occurs when the absolute value of the decay amplitude for D to decay to a final state f (A_f) is different from the one of corresponding CP -conjugated amplitude (“direct CPV ”). This can happen if the decay amplitude can be broken into at least two parts associated with different weak and strong phases,

$$A_f = |A_1| e^{i\delta_1} e^{i\phi_1} + |A_2| e^{i\delta_2} e^{i\phi_2}, \quad (34)$$

where ϕ_i represent weak phases ($\phi_i \rightarrow -\phi_i$ under CP -transformation), and δ_i represents strong phases ($\delta_i \rightarrow \delta_i$ under CP -transformation). This ensures that CP -conjugated amplitude, $\bar{A}_{\bar{f}}$ would differ from A_f .

- (II) CPV in $D^0 - \bar{D}^0$ mixing matrix. Introduction of $\Delta C = 2$ transitions, either via SM or NP one-loop or tree-level NP amplitudes leads to non-diagonal entries in the $D^0 - \bar{D}^0$ mass matrix,

$$\left[M - i\frac{\Gamma}{2} \right]_{ij} = \begin{pmatrix} A & p^2 \\ q^2 & A \end{pmatrix} \quad (35)$$

This type of CPV is manifest when $R_m^2 = |p/q|^2 = (2M_{12} - i\Gamma_{12})/(2M_{12}^* - i\Gamma_{12}^*) \neq 1$.

- (III) CPV in the interference of decays with and without mixing. This type of CPV is possible for a subset of final states to which both D^0 and \bar{D}^0 can decay.

For a given final state f , CP -violating contributions can be summarized in the parameter

$$\lambda_f = \frac{q}{p} \frac{\bar{A}_f}{A_f} = R_m e^{i(\phi_f + \delta)} \left| \frac{\bar{A}_f}{A_f} \right|, \quad (36)$$

where A_f and \bar{A}_f are the amplitudes for $D^0 \rightarrow f$ and $\bar{D}^0 \rightarrow f$ transitions respectively and δ is the strong phase difference between A_f and \bar{A}_f . Here ϕ represents the convention-independent weak phase difference between the ratio of decay amplitudes and the mixing matrix.

Most of the experimental techniques that are sensitive to CPV make use of decay asymmetries, which are similar to the ones employed in B-physics (139, 140, 141),

$$a_f = \frac{\Gamma(D \rightarrow f) - \Gamma(\bar{D} \rightarrow \bar{f})}{\Gamma(D \rightarrow f) + \Gamma(\bar{D} \rightarrow \bar{f})}. \quad (37)$$

One can also introduce a related asymmetry,

$$a_{\bar{f}} = \frac{\Gamma(D \rightarrow \bar{f}) - \Gamma(\bar{D} \rightarrow f)}{\Gamma(D \rightarrow \bar{f}) + \Gamma(\bar{D} \rightarrow f)}. \quad (38)$$

For charged D -decays the only contribution to the asymmetry of Eq. (37) comes from the multi-component structure of the $\Delta C = 1$ decay amplitude of Eq. (34). In this case,

$$\begin{aligned} a_f &= \frac{2\text{Im}(A_1 A_2^*) \sin \delta}{|A_1|^2 + |A_2|^2 + 2\text{Re}A_1 A_2^* \cos \delta} \\ &= 2r_f \sin \phi_f \sin \delta, \end{aligned} \quad (39)$$

where $\delta = \delta_1 - \delta_2$ is the CP -conserving phase difference and ϕ is the CP -violating one. $r_f = |A_2/A_1|$ is the ratio of amplitudes. Both r_f and δ are extremely difficult to compute reliably in D -decays. However, the task can be significantly simplified if one only concentrates on detection of NP in CP -violating asymmetries in the current round of experiments (142), i.e. at the $\mathcal{O}(1\%)$ level. This is the level at which a_f is currently probed experimentally. As follows from Eq. (39), in this case one should expect $r_f \sim 0.01$.

It is easy to see that the SM asymmetries are safely below this estimate. First, Cabibbo-favored ($A_f \sim \lambda^0$) and doubly Cabibbo-suppressed ($A_f \sim \lambda^2$) decay modes proceed via amplitudes that share the same weak phase, so no CP -asymmetry is generated². Moreover, presence of NP amplitudes does not significantly change this conclusion (96). On the other hand, singly-Cabibbo-suppressed decays ($A_f \sim \lambda^1$) readily have two-component structure, receiving contributions from both tree and penguin amplitudes. In this case the same conclusion follows from the consideration of the charm CKM unitarity,

$$V_{ud}V_{cd}^* + V_{us}V_{cs}^* + V_{ub}V_{cb}^* = 0. \quad (40)$$

In the Wolfenstein parametrization of CKM , the first two terms in this equation are of the order $\mathcal{O}(\lambda)$ (where $\lambda \simeq 0.22$), while the last one is $\mathcal{O}(\lambda^5)$. Thus, CP -violating asymmetry is expected to be at most $a_f \sim 10^{-3}$ in the SM. Model-dependent estimates of this asymmetry exist and are consistent with this estimate (143). Other observables are also possible, such as untagged CP -asymmetry (144), which for some final states can be written in terms of experimentally-measured quantities only, i.e. which suffers no theoretical uncertainties.

5.4 Experimental Considerations

A number of experimental realities prevented positive evidence for $D^0\overline{D}^0$ mixing until last year when sample sizes, with sufficiently small backgrounds finally became available (124, 145). Among the most important was that the mixing rate was very small ($R_M = (x_D^2 + y_D^2)/2 \sim 10^{-3}$) and mixing effects were greatest at about two lifetimes where sample sizes were quite depleted. Backgrounds were high and use of the two way constraint on both invariant mass M of the decay products of the D^0 and the difference, ΔM between M and the D^* invariant mass used to tag the D^0 flavor was necessary to suppress these. Cuts in data samples aimed at removing D^0 's from B decays that adversely affect decay time distributions also ate into sample sizes. Also, the D^0 lifetime (~ 400 fs) was small on the scale of measured decay times t and their uncertainties δt and large samples were required to properly understand their resolutions and the time offsets arising from detector alignment issues.

²Technically, there is a small, $\mathcal{O}(\lambda^4)$ phase difference between the dominant tree T amplitude and exchange E amplitudes.

5.5 Experimental Studies of $D^0 - \bar{D}^0$ Mixing

Studies of $D^0 - \bar{D}^0$ mixing mostly use samples of D^0 mesons whose flavor is identified by the sign of the “slow pion” π_s in the decay of a $D^{*+} \rightarrow D^0 \pi_s^+$. Effects of mixing in the subsequent decays are then examined in one of two alternative ways. Studies of time-dependent decay rates look either for structure in the “wrong sign” (WS) hadronic final states or for differences between the lifetimes of decays to CP eigenstates and to states of mixed CP . Alternatively, time-integrated rates are studied looking for decays either to semi-leptonic final states with the WS lepton,³ or for the effects upon rates resulting from quantum correlations between $D^0 - \bar{D}^0$ systems produced in $\psi(2S)$ decays at CLEOc.

5.6 Time-Dependent Studies

Mesons produced at time $t = 0$ as $D^0(\bar{D}^0)$ have amplitudes for decay to final state $f(\bar{f})$ at time t given by:

$$\begin{aligned} \langle f|H|D^0(t) \rangle &= e^{-(\Gamma_D + iM_D)t} A_f \left[\cosh\left((y_D + ix_D)\frac{\Gamma_D t}{2}\right) + \lambda_f \sinh\left((y_D + ix_D)\frac{\Gamma_D t}{2}\right) \right] \\ \langle \bar{f}|H|\bar{D}^0(t) \rangle &= e^{-(\Gamma_D + iM_D)t} \bar{A}_{\bar{f}} \left[\lambda_{\bar{f}}^{-1} \sinh\left((y_D + ix_D)\frac{\Gamma_D t}{2}\right) + \cosh\left((y_D + ix_D)\frac{\Gamma_D t}{2}\right) \right] \end{aligned} \quad (41)$$

where $\lambda_f = \frac{q\bar{A}_f}{pA_f}$ is defined in Eq. (36), M_D and Γ_D are the mean mass and width of the D_1 and D_2 and A_f and $\bar{A}_{\bar{f}}$ are amplitudes describing, respectively, the direct decays of D^0 and \bar{D}^0 to final state f .

In the absence of CPV in either mixing or direct decay to f , then $\lambda_f = e^{i\delta}$ where δ is the strong phase difference between $D^0 \rightarrow f$ and $\bar{D}^0 \rightarrow f$ amplitudes. With CPV in mixing ($p \neq q$) or in direct decay ($|\bar{A}_{\bar{f}}/A_f| \neq 1$), λ_f will be complex with weak phase ϕ_f and a strong phase δ .

Decay rates, proportional to the square modulus of these amplitudes provide information on x_D and y_D , only if the strong phase δ is known. This is, however, zero in the important special case when f is a CP eigenstate. In that case, if f has $CP = \eta$ the direct decay amplitudes are related by $A_\eta = \eta \bar{A}_\eta$, so that $\delta = 0$.

5.6.1 RESULTS FROM $D^0 \rightarrow K^+ \pi^-$ DECAYS. These WS decays can take place in two ways - either directly, by a doubly Cabibbo suppressed (DCS) mechanism or by mixing ($D^0 \rightarrow \bar{D}^0$) followed by “right sign” (RS) Cabibbo favored (CF) decay $\bar{D}^0 \rightarrow K^+ \pi^-$. These two processes interfere giving the time-dependent decay amplitudes given in Eqs. (41). Neglecting CPV and assuming that $|x_D|$ and $|y_D| \ll 1$, this leads to the decay rate R_{WS} for these decays

$$\frac{R_{WS}(t)}{e^{-\Gamma_D t}} \propto R_D + \sqrt{R_D} y' t + R_M (\Gamma_D t)^2 / 2 \quad (42)$$

R_D is the DCS decay rate alone, in the absence of mixing, R_M is the mixing rate and the middle term, linear in y' , results from interference between mixing and DCS amplitudes. Deviation from a purely exponential decay, expressed in the

³Actually, the signal for WS decays also do use information from the time-dependence from mixed decays to distinguish them the backgrounds.

right side of Eq. (42), can provide information on x'^2 and y' , but not the values of x_D and y_D or their relative signs.

This method has been used a number of times, in E691 and E791 (fixed target experiments at Fermilab), by BABAR and by CLEO using 9 fb^{-1} of e^+e^- collisions at $\sqrt{s} \approx 10 \text{ GeV}$ (146). The most stringent limit on $D^0\bar{D}^0$ mixing using this method is reported by Belle (149). Recently, however, using a 384 fb^{-1} data sample, the BABAR collaboration finally reported evidence for mixing from their sample of $4,030 \pm 90$ decays of D^0 mesons to the WS final state.

The distribution in decay times t (uncertainty δt) for these D^0 and \bar{D}^0 events is shown in Fig. 6(a). Also shown are the projections onto the time axis of fits made in the $(M, \Delta M, t, \delta t)$ distribution for events near the D^0 signal region. The dashed curve shows a fit made on the assumption that $x'^2 = y' = 0$ and the solid curve represents a fit where these parameters are allowed to float. Precise knowledge of parameters describing the distribution of δt , clearly an important component in these fits, is obtained from a sample of $\sim 1.3 \times 10^6$ “right sign” (RS) candidates for the Cabibbo favored decays $D^0 \rightarrow K^-\pi^+$. The difference between the fit with mixing and that without is significant as seen from the residuals in Fig. 6(b) and in the ratio of WS to RS decays in Fig. 6(c). The central values from the mixing fit occur at a negative (unphysical) value for x'^2 . The likelihood obtained in the fit at the point ($x'^2 = 0, y' = 6.4 \times 10^{-3}$) just inside the physical region differs from that at the central point by only 0.7 units, while the likelihood at the no mixing point ($x'^2 = y' = 0$) differs by almost 24 units. This difference is taken to indicate evidence for mixing at $3.9\sigma'$ significance. The CDF experiment, using data from a 1.5 fb^{-1} $\bar{p}p$ exposure at $\sqrt{s} = 1.96 \text{ TeV}$, has recently confirmed the BABAR result at a significance of 3.8 standard deviations (147). These results are also summarized in Table 9, where it is seen that agreement with BABAR is excellent. In this experiment, it is not possible to remove background from D mesons from B decays simply with a momentum cut, as in the BABAR and Belle experiments. This is, however, identified from its vertex distribution and properly taken into account in their analysis. In an earlier analysis, the Belle collaboration (149) also obtained results with greater precision than either the BABAR or CDF measurements. Their central values for x'^2 and y' , however, were closer to zero and so did not provide convincing evidence for mixing and only 95% confidence limits could be reported.

Table 9 summarizes the data on mixing derived from this hadronic channel. Generally, the highest sensitivity is achieved with fits assuming CP violation. Note that the parameters x' and y' include a strong phase δ , the phase of the amplitude ratio $\langle K^+\pi^- | D^0 \rangle / \langle K^+\pi^- | \bar{D}^0 \rangle$.

5.6.2 LIFETIME DIFFERENCE MEASUREMENTS. The Belle collaboration also presented evidence for mixing using a 540 fb^{-1} e^+e^- data at the $\Upsilon(4S)$. They measured lifetimes for singly Cabibbo-suppressed decays to the $CP = +1$ final states K^+K^- and $\pi^+\pi^-$ and for Cabibbo-favored decays to the final state $K^-\pi^+$ with mixed CP (145).

This method was first used by the E791 collaboration (150) who were unable to detect mixing due to limited statistical precision. Subsequently, upper limits were reported by FOCUS, and CLEO. In the approximation that x_D and y_D are small, decays to $CP = +1$ eigenstates follow approximately exponential forms

with lifetimes (125), respectively, for decays of D^0 and \bar{D}^0 of

$$\begin{aligned}\tau^+ &= \tau^0 [1 + |q/p|(y \cos \phi_f - x \sin \phi_f)]^{-1} \\ \tau^- &= \tau^0 [1 + |p/q|(y \cos \phi_f + x \sin \phi_f)]^{-1}\end{aligned}\quad (43)$$

where τ^0 is the lifetime for decays to non- CP eigenstates such as $K^-\pi^+$. For such measurements, it is convenient to define

$$\Delta Y = (\tau^0 / \langle \tau \rangle) a_\tau \quad (44)$$

where $\langle \tau \rangle$ is the average of τ^+ and τ^- and $a_\tau = (\tau^- - \tau^+) / (\tau^- + \tau^+)$ is their asymmetry. In the absence of mixing ($x = y = 0$) both are zero. In the absence of CPV in mixing or in decay (i.e. $\phi_f = 0$) then $\Delta Y = 0$ and $y_D^{CP} = y$.

These measurements require that backgrounds are small and have a well understood time-dependence. The Belle samples, consisting of 111K K^+K^- , 1.22×10^6 $K^-\pi^+$ and 49K $\pi^+\pi^-$ with purities 98% and 99% and 92% purity, respectively. The decay times for these were fit simultaneously to distributions with an exponential for each signal convolved with the time resolution function over the expected background distributions.

Estimates for y_D^{CP} were made using both D^0 and \bar{D}^0 samples together and for τ^+ and τ^- from separate fits to each. The major systematic uncertainties were from an understanding of time offsets and from possible t -dependence of the efficiency for reconstructing events. The result obtained

$$\begin{aligned}y_D^{CP} &= (1.31 \pm 0.32 \pm 0.25)\% \\ a_\tau &= (0.01 \pm 0.30 \pm 0.15)\%\end{aligned}$$

shows that y_D^{CP} is not zero, evidence for mixing at the 3.2σ level. However, a_τ is consistent with zero, so there is no evidence for CPV .

A similar analysis by BABAR, using a 384 fb^{-1} data set, confirms these results (145). Though the BABAR sample is smaller, a higher purity is achieved. Their results

$$\begin{aligned}y_D^{CP} &= (1.24 \pm 0.39 \pm 0.13)\% \\ \Delta Y &= (-0.26 \pm 0.36 \pm 0.08)\%\end{aligned}$$

agree well with Belle's, and show evidence for mixing at the 3.0σ level, but with no evidence for CPV .

5.6.3 MIXING IN THE DECAYS $D^0 \rightarrow K_S \pi^+ \pi^-$. For $D^0 \rightarrow K_S \pi^+ \pi^-$, the time dependence of the Dalitz plot distribution allows one to measure x_D and y_D directly. This technique was first developed by the CLEO collaboration (151), who used a 9 fb^{-1} data sample. Assuming no CPV , they obtained the limits $(-4.7 < x < 8.6)\%$ and $(-6.1 < y < 3.5)\%$ at 95 % confidence level.

A special feature of this decay mode is that, treating K_S as a $CP = +1$ eigenstate, final states f reached via the $\pi\pi$ channel are also CP eigenstates for which the strong phase difference $\delta = 0$. This provides a reference phase for a time-dependent Dalitz plot analysis that will determine the A_f, \bar{A}_f for all channels everywhere in the plot. Thus, these decays allow measurement of x_D, y_D and their relative sign, free from any unknown strong phase. This fit can also provide magnitude and phase of the λ_f 's, providing a test for CPV .

Belle applied this technique to a data sample 60 times larger. The $K_S \pi^+ \pi^-$ Dalitz plot is shown in Fig. 7, where the RS K^{*-} form a vertical band and

ρ^0 is the diagonal band. The WS K^{*+} appears as a weak, horizontal band destructively interfering with other structures in the plot. It is expected that RS and WS K^* amplitudes should have opposite signs since their weak CF or DCS phases differ in sign. An isobar model description of the amplitudes A_f is used, writing them as sums of Breit-Wigner functions and spin factors, with complex coefficients determined in the fit as in Eq. (20). For the Belle data, 18 isobars, including ρ - ω mixing, two $\pi^+\pi^-$ S -wave states and a non-resonant term NR were required to provide a reasonable match to all the features seen. The appropriate time-dependencies were included as in Eq. (41).

Three fits were made. In one, no CPV is included (all D^0 and \overline{D}^0 events were combined and isobar coefficients for D^0 set to equal those for \overline{D}^0). The condition $p = q$ is also imposed. In the other fit these conditions were relaxed, introducing a set of complex isobar coefficients for \overline{D}^0 differing from those for D^0 . The modulus and phase of the ratio p/q were also allowed to float. In the last fit, CPV in mixing ($p \neq q$) is allowed but direct CPV is not (isobar coefficients constrained to be the same for D^0 as for \overline{D}^0). The results of these three fits are summarized in Table 10.

The authors estimate that the best solution differs from the mixing point ($x_D = y_D = 0$) by 2.2 standard deviations. Allowing for CP violation, they obtain the CPV parameters $|q/p| = 0.86_{-0.29}^{+0.30+0.06} \pm 0.08$ and $\arg(q/p) = (-14_{-18-3-4}^{+16+5+2})^\circ$. This result does not establish evidence for mixing nor for CPV . It does, however, illustrate a powerful way to study mixing, able to determine x_D , y_D and their relative signs, and the CPV parameters ϕ and $|p/q|$.

5.7 Time Independent Studies.

Rates for WS leptons in semi-leptonic decays, a clear signal for mixing, could directly determine the mixing rate R_M . So far, with samples available, these have only been able to produce upper limits on this quantity. The most precise limits are from Belle (152), from a 253 fb^{-1} sample, and from BABAR (153) with a 344 fb^{-1} sample. The BABAR analysis differed considerably from Belle's in that they adopted a double tagging approach, requiring a fully reconstructed D on the side opposite the semi-leptonic decay, used to reduce WS backgrounds. Event yields differed by orders of magnitude between the two experiments, yet the limits obtained were very similar:

$$\begin{array}{ll} \text{Belle} & R_M < 1 \times 10^{-3} \\ \text{BABAR} & (-1.3 < R_M < +1.2) \times 10^{-3} \end{array}$$

CLEO-c can exploit the quantum coherence of the $D^0\overline{D}^0$ produced via the $\psi(3770)$ resonance to extract several important variables affecting $D^0\overline{D}^0$ mixing. The pair is produced in a $C = -1$ state, while $C = +1$ states are accessible at a higher energy, if $\gamma D^0\overline{D}^0$ final states can be tagged. By reconstructing one neutral D meson into a CP eigenstate decay mode, the CP eigenvalue must be the opposite for C odd wave functions, and the same for C even wave functions (154, 155), assuming no CPV . All the mixing observables can, in principle, be measured. A sophisticated fitting technique has been developed (156) to reach maximum sensitivity. For decays of $\psi(3770)$ to $D^0 - \overline{D}^0$ pairs (157, 158), the D^0 's, in a coherent P -wave state, and with opposite flavor and CP , decay in a correlated

way so that $K^-\pi^+$ rates depend upon R_M, R_D, y' and δ , the strong phase difference between amplitudes for CF and DCS decays. Using their 281 pb^{-1} data sample collected at the $\psi(3770)$, CLEO determines $\cos \delta = 1.03_{-0.17}^{+0.31} \pm 0.06$ (159).

5.7.1 AVERAGING THE RESULTS. The decays discussed above provide information in different forms, depending upon the final state. Semi-leptonic modes determine R_M , WS hadronic systems measure x'^2 and y' separately for D^0 and \bar{D}^0 . Decays to CP eigenstates measure y_D^{CP} and ΔY and quantum correlated states from $\psi(3770) \rightarrow D^0$ decays can measure R_M, R_D, y_D and $\cos \phi$ for various hadron systems. Parameters $x_D, y_D, |p/q|$ and $\arg p/q$ are obtained from time dependence amplitude analyses of decays of D^0 to final states with more than two hadrons, as long as those amplitudes include at least one CP eigenstate.

The parameters of physics interest that define values for all these quantities include $x_D, y_D, |p/q|, \arg p/q, \phi_{K\pi}^{WS}, \phi_{K\pi}^{WS}, R_D$ and its asymmetry $a_D = (R_D - \bar{R}_D)/(R_D + \bar{R}_D)$. The Heavy Flavor Averaging Group (HFAG) made a χ^2 fit to obtain values for these parameters that best describe all 26 available observations. (160) Results, projected onto the (x_D, y_D) and $(|p/q|, \arg p/q)$ planes in Fig. 8.

The point at which there is no mixing on the (x_D, y_D) plane lies at the origin, outside the 5σ contour. This indicates very strong evidence for $D^0 - \bar{D}^0$ mixing. There is no evidence, however, for CPV in the mixing. The point where $p = q$ in the $(|p/q|, \arg p/q)$ plane lies at $(1, 0)$, right on the 1σ contour.

Evidence for mixing is convincing and different experiments and methods agree well. Since $y_D^{CP} > 0$, then the $CP = -1$ state has longer lifetime, as in the other neutral mesons that mix. If the sign of x_D/y_D remains positive as more measurements are made, then the $CP = -1$ state is lighter, unlike the K^0 system. Finally, there is no evidence for CPV so far.

5.7.2 RESULTS OF EXPERIMENTAL SEARCHES FOR CPV . At the present time, there is no experimental evidence for CPV in weak decays in the charm sector. Finding it in CF or DCS decay modes would signal possible NP. For decays to multi-body systems, the decay asymmetry could appear only in certain sub channels and result in particle-antiparticle differences in phase space distribution. Searches may also be made for T -violation.

5.7.3 ASYMMETRIES IN TIME-INTEGRATED PARTIAL WIDTHS. Until this year, measurements of the asymmetries in partial widths for time-integrated D decay rates were known with precisions of a few percent. A recent compilation of average values (161) for D decay asymmetries for a number of modes measured by CDF, FOCUS, E791, CLEO, BABAR and Belle are summarized in Table 11. They are all consistent with zero, with a precision of a few % in most cases. Included in the most recent results are measurements from CLEOc (6) of CF modes using their $\psi(3770)$ data. Precisions were excellent, of order 1%.

The most precise measurement comes from BABAR (162) with a precision of 0.34%, for the decays $D^0 \rightarrow K^+K^-$ and of 0.5% for $D^0 \rightarrow \pi^+\pi^-$. This precision required careful consideration of systematic effects, notably charge and tagging asymmetries calibrated using data from the $K^-\pi^+$ CF mode. Effects from forward-backward production asymmetry arising from higher order QED were also taken into account. Systematic uncertainties were 0.13% for K^+K^- and 0.22% for $\pi^+\pi^-$, so the results were limited by statistics. Nevertheless, finding CPV closer to 0.1% in CS modes, and less in CF or DCS modes (the goals to observe NP) will require even better precision.

CPV effects would influence the Dalitz plot distributions in three-body decays

such as $D^0 \rightarrow \pi^+\pi^-\pi^0$ since asymmetries would affect different partial waves in each of the three channels in differing degrees. Such effects would also be expected to introduce phase differences between D^0 and \bar{D}^0 , and these could be observed in analysis of the Dalitz plots. (113) found no such effects at the few % level. A model-independent approach might be interesting to pursue - possibly by the B factories where an order of magnitude more data is available. An isobar model analysis of this mode by CLEOc sees no effect at the few percent level.

5.7.4 T -VIOLATION STUDIES. It has been pointed out (139) that T -violation in charmed meson decays may also be observed in the asymmetry of triple scalar products (T -odd) of the momenta of the particles emerging from 4-body decays (139). The only such measurements to date are from the FOCUS collaboration (163), who measured the quantities (defined in terms of momenta \vec{p} with suffices indicating each product from 4-body D^0 , \bar{D}^0 and D_s^+ decays)

$$\begin{aligned} C_T &= \vec{p}_{K^+} \cdot (\vec{p}_{\pi^+} \times \vec{p}_{\pi^-}) \\ A_T &= \frac{\Gamma(C_T > 0) - \Gamma(C_T < 0)}{\Gamma(C_T > 0) + \Gamma(C_T < 0)} \end{aligned}$$

The conjugate quantities (\bar{C}_T and \bar{A}_T) for \bar{D}^0 , D^- and D_s^- decays were also measured. The modes studied were $D^0 \rightarrow K^+K^-\pi^+\pi^-$, $D^+ \rightarrow K^+K_S\pi^+\pi^-$ and $D_s^+ \rightarrow K^+K_S\pi^+\pi^-$. Any asymmetry not consistent with zero would indicate T -violation in the absence of strong interactions. The latter introduce the same asymmetries in particle and anti-particle decay, so the quantity $A_{T\text{-viol}} = (1/2)(A_T - \bar{A}_T)$, which would be zero if T is conserved, is evaluated

$$\begin{aligned} D^0 \rightarrow K^+K^-\pi^+\pi^- & 0.010 \pm 0.057 \pm 0.037 \\ D^+ \rightarrow K^+K_S\pi^+\pi^- & 0.023 \pm 0.062 \pm 0.022 \\ D^0 \rightarrow K^+K^-\pi^+\pi^- & -0.036 \pm 0.067 \pm 0.023 \end{aligned}$$

all consistent with zero.

5.7.5 SUMMARY. Clearly, experimental precision is not yet sufficient to challenge the SM with respect to its predictions of CPV in the charm sector. The outlook is, however, good since the precision of asymmetry measurements is not yet limited by systematics. Also, model-independent studies of the multi-body channels $\pi^+\pi^-\pi^0$ and $K^+K^-\pi^0$, less prone to systematic uncertainties, show promise as a tool for observing effects of CPV .

Both BABAR and Belle still have large samples of 4-body decays where T -violation tests similar to that made by FOCUS can be repeated. Also, more data is to come from both B factories on the K^-K^+ and $\pi^-\pi^+$ channels where the precisions are beginning to become interesting. Even larger samples from charm factories, LHCb, or, possibly, Super B factories in Italy or at KEK might produce a definitive answer on NP manifest in these studies.

6 CONCLUSIONS AND OUTLOOK

Charm decays remain an exciting field for both theoretical and experimental investigations. Charm quark transition amplitudes, described in this review, represent a crucial tool to understand strong interaction dynamics in the non-perturbative regime. Complementary information that constrains model building and lattice gauge calculations is coming from the rich spectroscopy of charmed

mesons and baryons, which is beyond the scope of this review. The validation of theoretical tools that tackle non-perturbative processes is critical to precision tests of the Yukawa sector of the SM, in particular to unitarity checks of the Cabibbo-Kobayashi-Maskawa matrix.

Finally, charm decays provide a unique window on NP, provided it affects u -type quark dynamics. This way charm phenomenology can have an impact on the interpretation of results from the direct searches for new physics to be performed at the LHC. Charm quark is the only u -type quark that can have flavor oscillations. Thus the observation of $D^0\bar{D}^0$ mixing is already constraining many scenarios of physics beyond the SM. In addition, a multitude of new physics models predict enhancements on CP violating phases in D decays, beyond the 10^{-3} level generally predicted within the SM. A full exploration of CPV in the charm sector, that hopefully will be achieved in the next decade, is a critical ingredient to further narrow the vast parameter space presently characterizing all the new physics models.

7 ACKNOWLEDGMENTS

The authors would like to thank their colleagues at their institutions for helpful conversations during the course of writing of this review, and especially D. Asner, D. Cinabro, R. Harr, S. Pakvasa, A. Schwartz, and S. Stone for careful reading of the manuscript and useful comments. The work of M.A. was supported in part by the U.S. National Science Foundation under Grant PHY-0553004. B.M. was supported by the U.S. National Science Foundation under Grant PHY-0457336. A.A.P. was supported in part by the U.S. National Science Foundation CAREER Award PHY-0547794, and by the U.S. Department of Energy under Contract DE-FG02-96ER41005.

LITERATURE CITED

1. Gaillard MK, Lee BW, Rosner JL. *Rev. Mod. Phys.* 47:277 (1975)
2. Petrov AA., hep-ph/0311371
3. Adler J *et al.* (Mark III collaboration) *Phys. Rev. Lett.* **60**, 89 (1988).
4. Briere RA *et al.*, Preprint CLNS-01-1742
5. Li WG (BES collaboration), *Int. J. Mod. Phys. A* **20**, 1560 (2005).
6. Dobbs S, *et al.* arXiv:0709.3783 [hep-ex]
7. Widhalm L, *et al.* *Phys. Rev. Lett.* 97:061804 (2006)
8. Albini E, *et al.* *Phys. Lett.* 110B:339 (1982)
9. Artuso M, *Vertex 2007 Proceedings* (2008)
10. Aubin C, *et al.* *Phys. Rev. Lett.* 95:122002 (2005)
11. Follana E, Davies CTH, Lepage GP, Shigemitsu J. arXiv:0706.1726 [hep-lat]
12. Aubin C, *et al.* *Phys. Rev. Lett.* 94:011601 (2005)
13. Shifman MA, Vainshtein AI, Zakharov VI. *Nucl. Phys.* B147:385 (1979)
14. Narison S. hep-ph/0202200
15. Rosner J L and Stone S, hep-ex/0802.1043 (2008)
16. Scora D, Isgur N. *Phys. Rev.* D52:2783 (1995)
17. Isgur N and Wise M B, *Phys. Lett.* B232:113 (1989)
18. Isgur N and Wise M B, *Phys. Rev.* D42:2388 (1990)
19. Grinstein B, Pirjol D, *Phys. Rev.* D70:114005 (2004)

20. Chiu W T, et al. *Phys. Lett.* B624:31 (2005)
21. Lellouch L and Lin C J, *Phys. Rev.* D64:094501 (2005)
22. Becirevic D, *Phys. Rev.* D60:074501 (1999)
23. Bordes J, Penarrocha J, and Schilcher K, *JHEP* 0522:014 (2005)
24. Narison S, hep-ph/0202200
25. Badalian AM, et al. *Phys. Rev.* D75:116001 (2007); see also Badalian AM and Bakker BLG, hep-ph/0702229
26. Amundson J, *Phys. Rev.* D47:3059 (1993)
27. Artuso M, et al. *Phys. Rev. Lett.* 95:251801 (2005)
28. Aubert B, et al. *Phys. Rev. Lett.* 98:141801 (2007)
29. Hewett JL, hep-ph/9505246
30. Ikado K et al., *Phys. Rev. Lett.* 97:251802 (2006)
31. Coan TE et al., *Phys. Rev. Lett.* 95:191802 (2005); Huang GS et al., *Phys. Rev. Lett.* 95:101801 (2005)
32. Ablikim M, et al., *Phys. Lett.* B608:24 (2005); Ablikim M et al., *Phys. Lett.* B597:39 (2004)
33. Yao WM, et al. *J. Phys.* G33:1 (2006), see also <http://pdg.lbl.gov>
34. Artuso M, et al. *Phys. Rev. Lett.* 99:071802 (2007)
35. Ecklund KM. arXiv:0712.1175 [hep-ex]
36. Abe K, et al. arXiv:0709.1340 [hep-ex]
37. Chadha M, et al. *Phys. Rev.* D58:032002 (1998)
38. Alexandrov Y, et al. *Phys. Lett.* B478:31 (2000)
39. Heister A, et al. *Phys. Lett.* B528:1 (2002)
40. Acciarri M, et al. *Phys. Lett.* B396:327 (1997)
41. Abbiendi G, et al. *Phys. Lett.* B516:236 (2001)
42. Adam N et al., *Phys. Rev. Lett.* 97:251801 (2006)
43. Stone S. *AIP Conf. Proc.* 842:253 (2006)
44. Boyd CG, Grinstein B, Lebed RF. *Phys. Rev.* D56:6895 (1997)
45. Becirevic D, Kaidalov AB. *Phys. Lett.* B478:417 (2000)
46. Link JM et al. *Phys. Lett.* B607:233 (2005)
47. Nierste U, *Int. J. Mod. Phys.* A21:1724 (2005)
48. <http://lepewwg.web.cern.ch/LEPEWWG/lepww/4f/Winter05/>
49. Cronin-Hennessy D, et al. arXiv:0712.0998 [hep-ex]
50. Becher T, Hill RJ. *Phys. Lett.* B633:61 (2006)
51. Link JM, et al. *Phys. Lett.* B607:233 (2005)
52. Pavlunin V. *PoS HEP2005:206* (2006)
53. Aubert B, et al. arXiv:0704.0020 [hep-ex]
54. Huang GS, et al. *Phys. Rev. Lett.* 94:011802 (2005)
55. Link JM, et al. *Phys. Lett.* B633:183 (2006)
56. Shepherd MR, et al. *Phys. Rev.* D74:052001 (2006)
57. Fajfer S, Kamenik JF. *Phys. Rev.* D73:057503 (2006)
58. Link JM, et al. *Phys. Lett.* B535:43 (2002)
59. Bianco S, Fabbri FL, Benson D, Bigi I. *Riv. Nuovo Cim.* 26N7:1 (2003)
60. Glashow SL, Iliopoulos J, Maiani L. *Phys. Rev.* D2:1285 (1970)
61. Burdman G, Golowich E, Hewett JL, Pakvasa S. *Phys. Rev.* D52:6383 (1995)
62. Burdman G, Golowich E, Hewett JL, Pakvasa S. *Phys. Rev.* D66:014009 (2002)
63. Fajfer S, Kosnik N, Prelovsek S. *Phys. Rev.* D76:074010 (2007)
64. He Q, et al. *Phys. Rev. Lett.* 95:221802 (2005)
65. Abe K et al., *Phys. Rev. Lett.* 92:101803 (2004)

66. Acosta D et al., *Phys. Rev.* D68:091101 (2007)
67. Aubert B, et al. hep-ex/0607051
68. Abazov VM, et al. arXiv:0708.2094 [hep-ex]
69. Aubert B, et al. *Phys. Rev. Lett.* 93:191801 (2004)
70. Acosta DE, et al. *Phys. Rev.* D68:091101 (2003)
71. Freyberger A, et al. *Phys. Rev. Lett.* 76:3065 (1996)
72. Cavoto G, et al. hep-ph/0603019
73. Aubert B, et al. *Phys. Rev.* D71:032005 (2005)
74. Giri A, Grossman Y, Soffer A, Zupan J. *Phys. Rev.* D68:054018 (2003)
75. Abe K, et al. *Phys. Rev. Lett.* 99:131803 (2007)
76. Buccella F, et al. *Phys. Rev.* D51:3478 (1995)
77. Bauer M, Stech B, Wirbel M. *Z. Phys.* C34:103 (1987)
78. Buras AJ, Gerard JM, Ruckl R. *Nucl. Phys.* B268:16 (1986)
79. Blok B, Shifman MA. *Nucl. Phys.* B399:441 (1993)
80. Falk AF, Nir Y, Petrov AA. *JHEP* 12:019 (1999)
81. Savage MJ. *Phys. Lett.* B257:414 (1991)
82. Dobbs S, et al. arXiv:0709.3783 [hep-ex]
83. Alexander J, et al. arXiv:0801.0680 [hep-ex].
84. Baltrusaitis RM, et al. *Phys. Rev. Lett.* 56:2140 (1986)
85. Sun WM. *Nucl. Instrum. Meth.* A556:325 (2006)
86. Aubert B, et al. arXiv:0704.2080 [hep-ex]
87. Abe K, et al. hep-ex/0701053
88. White E, He Q. arXiv:0711.2285 [hep-ex]
89. Bigi IY, Yamamoto H. *Phys. Lett.* B349:363 (1995)
90. Rosner JL. *Phys. Rev.* D74:057502 (2006)
91. Rubin P, et al. *Phys. Rev. Lett.* 96:081802 (2006)
92. Selen M, et al. *Phys. Rev. Lett.* 71:1973 (1993)
93. Aubert B, et al. *Phys. Rev.* D74:091102 (2006)
94. Abe K, et al. hep-ex/0610062
95. Adams GS, et al. *Phys. Rev. Lett.* 99:191805 (2007)
96. Bergmann S, Nir Y. *JHEP* 09:031 (1999)
97. Aubert B, et al. *Phys. Rev.* D74:011107 (2006)
98. Dytman SA, et al. *Phys. Rev.* D74:071102 (2006)
99. Meadows B. arXiv:0712.1605 [hep-ex]
100. Bondar A, Poluektov A. arXiv:0801.0840 [hep-ex]
101. Watson KM. *Phys. Rev.* 88:1163 (1952) a detailed discussion as well as a complete list of references can be found in 'Final State Interactions' by J. Gillespie, Holden-Day Publishers, San Francisco, (1964).
102. Link JM, et al. *Phys. Lett.* B653:1 (2007)
103. Blatt JM, Weisskopf VF. *Wiley, New York* :361 (1952)
104. Wigner E. P. *Phys. Rev.* 70:15 (1946)
105. Chung SU, et al. *Annalen Phys.* 4:404 (1995)
106. Anisovich VV, Sarantsev AV. *Eur. Phys. J.* A16:229 (2003)
107. Aitala EM, et al. *Phys. Rev.* D73:032004 (2006)
108. Muramatsu H, et al. *Phys. Rev. Lett.* 89:251802 (2002)
109. Poluektov A, et al. *Phys. Rev.* D73:112009 (2006)
110. Poluektov A, et al. *Phys. Rev.* D70:072003 (2004)
111. Aubert B, et al. *Phys. Rev. Lett.* 95:121802 (2005)
112. Aubert B, et al. hep-ex/0703037
113. Cronin-Hennessy D, et al. *Phys. Rev.* D72:031102 (2005)

114. Aubert B, et al. *Phys. Rev.* D72:052008 (2005)
115. Bonvicini G, et al. *Phys. Rev.* D76:012001 (2007)
116. Oller JA. *Phys. Rev.* D71:054030 (2005)
117. Schechter J. *Int. J. Mod. Phys.* A20:6149 (2005)
118. Aitala EM, et al. *Phys. Lett.* B404:187 (1997)
119. Aubert B, et al. *Phys. Rev.* D76:011102 (2007)
120. Aston D, et al. *Nucl. Phys.* B296:493 (1988)
121. Frabetti PL, et al. *Phys. Lett.* B351:591 (1995)
122. Pappagallo M. arXiv:0711.4769 [hep-ex]
123. Pais A, Treiman SB. *Phys. Rev.* D12:2744 (1975)
124. Aubert B, et al. *Phys. Rev. Lett.* 98:211802 (2007)
125. Bergmann S, et al. *Phys. Lett.* B486:418 (2000)
126. Falk AF, Grossman Y, Ligeti Z, , Petrov AA. *Phys. Rev.* D65:054034 (2002)
127. Georgi H. *Phys. Lett.* B297:353 (1992)
128. Ohl T, Ricciardi G, Simmons EH. *Nucl. Phys.* B403:605 (1993)
129. Petrov AA. *Phys. Rev.* D56:1685 (1997)
130. Bigi IY, Uraltsev NG. *Nucl. Phys.* B592:92 (2001)
131. Golowich E, Petrov AA. *Phys. Lett.* B625:53 (2005)
132. Donoghue JF, Golowich E, Holstein BR, Trampetic J. *Phys. Rev.* D33:179 (1986)
133. Colangelo P, Nardulli G, Paver N. *Phys. Lett.* B242:71 (1990)
134. Golowich E, Petrov AA. *Phys. Lett.* B427:172 (1998)
135. Falk AF, et al. *Phys. Rev.* D69:114021 (2004)
136. Golowich E, Hewett J, Pakvasa S, Petrov AA. *Phys. Rev.* D76:095009 (2007)
137. Golowich E, Pakvasa S, Petrov AA. *Phys. Rev. Lett.* 98:181801 (2007)
138. Petrov AA, Yeghiyan GK. arXiv:0710.4939 [hep-ph], *Phys. Rev. D.*, In press (2007)
139. Bigi IY, Sanda AI. *Camb. Monogr. Part. Phys. Nucl. Phys. Cosmol.* 9:1 (2000)
140. Petrov AA. arXiv:0711.1564 [hep-ph]
141. This asymmetry was first introduced in Brown T, Tuan SF, Pakvasa S. *Phys. Rev. Lett.* 51, 1823 (1983), and Bigi IY, Sanda AI. *Phys. Rev.* D29, 1393 (1984)
142. Grossman Y, Kagan AL, Nir Y. *Phys. Rev.* D75:036008 (2007)
143. Buccella F, et al. *Phys. Lett.* B302:319 (1993)
144. Petrov AA. *Phys. Rev.* D69:111901 (2004)
145. Staric M, et al. *Phys. Rev. Lett.* 98:211803 (2007)
146. Aitala E. et al. *Phys.Rev.* D57:13-27 (1998); Anjos, J, et al. *Phys.Rev.Lett.* 60:1239 (1988); Aubert B, et al. *Phys.Rev.Lett.* 91:171801 (2003); Godang R, et al. *Phys. Rev. Lett.* 84:5038 (2000)
147. Aaltonen T. arXiv:0712.1567 [hep-ex]
148. Aubert B et al. (BABAR Collaboration), arXiv:0712.2249 [hep-ex]
149. Zhang LM, et al. *Phys. Rev. Lett.* 96:151801 (2006)
150. Aitala EM, et al. *Phys. Rev. Lett.* 83:32 (1999)
151. Asner DM, et al. *Phys. Rev.* D72:012001 (2005)
152. Bitenc U, et al. *Phys. Rev.* D72:071101 (2005)
153. Aubert B, et al. *Phys. Rev.* D76:014018 (2007)
154. Gronau M, Grossman Y, Rosner JL. *Phys. Lett.* B508:37 (2001)
155. Atwood D, Petrov AA. *Phys. Rev.* D71:054032 (2005)
156. Asner DM, Sun WM. *Phys. Rev.* D73:034024 (2006)

157. Asner DM, et al. *Int. J. Mod. Phys. A*21:5456 (2006)
158. Sun WM. arXiv:0712.0498 [hep-ex]
159. Rosner J, et al. arXiv:0802.2264v1 [hep-ex]; Asner D, et al. arXiv:0802.2268v1 [hep-ex]
160. Schwartz A. http://www.slac.stanford.edu/xorg/hfag/charm/Beijing07/results_mix+cpv.html
161. Heavy Flavor Averaging Group (HFAG), <http://www.slac.stanford.edu/xorg/hfag/charm/>
162. Aubert B, et al. *Phys. Rev. Lett.* 100:061803 (2008)
163. Link JM, et al. *Phys. Lett.* B622:239 (2005)

Table 1: Theoretical predictions for $f_{D^+}, f_{D_s^+}, f_{D_s^+}/f_{D^+}$.

Authors	f_{D^+} (MeV)	$f_{D_s^+}$ (MeV)	$f_{D_s^+}/f_{D^+}$
Unquenched lattice calculations			
HPQCD+UKQCD (11)	208 ± 4	241 ± 3	1.162 ± 0.009
FNAL+MILC+HPQCD (10)	$201 \pm 3 \pm 17$	$249 \pm 3 \pm 16$	$1.24 \pm 0.01 \pm 0.07$
Quenched Lattice QCD Calculations			
Taiwan (20)	$235 \pm 8 \pm 14$	$266 \pm 10 \pm 18$	$1.13 \pm 0.03 \pm 0.05$
UKQCD (21)	$210 \pm 10^{+17}_{-16}$	$236 \pm 8^{+17}_{-14}$	$1.13 \pm 0.02^{+0.04}_{-0.02}$
Becirevic <i>et al.</i> (22)	$211 \pm 14^{+2}_{-12}$	$231 \pm 12^{+6}_{-1}$	1.10 ± 0.02
QCD sum rules and other approximations			
J. Bordes <i>et al.</i> (23)	177 ± 21	205 ± 22	$1.16 \pm 0.02 \pm 0.03$
S. Narison (24)	203 ± 10	235 ± 24	1.15 ± 0.04
Field Correlators (25)	210 ± 10	260 ± 10	1.24 ± 0.03
Isospin Splitting (26)		262 ± 29	

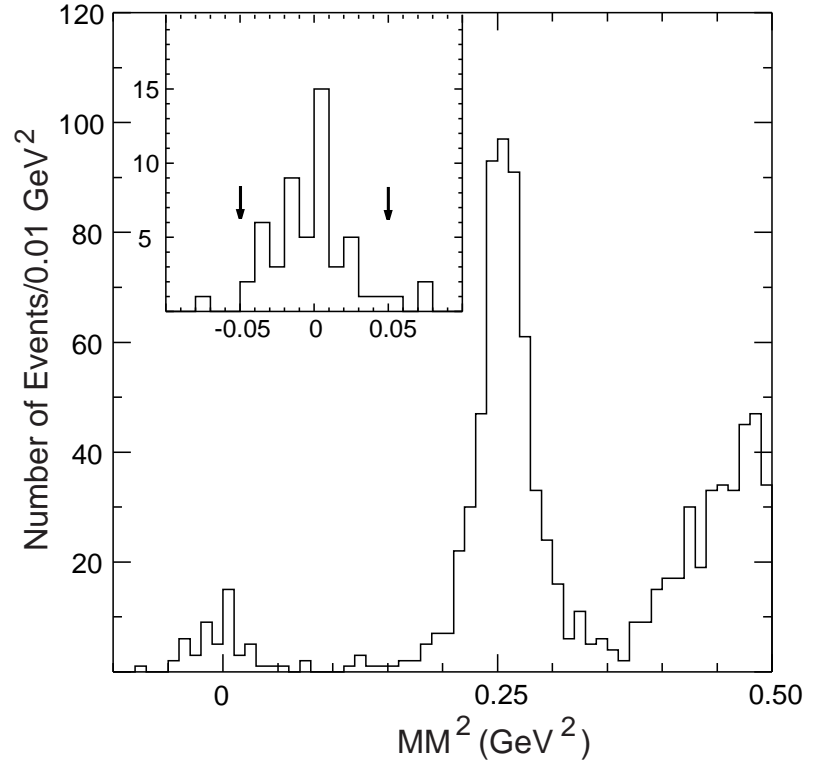


Figure 1: CLEO-c MM^2 using D^- tags and one opposite charged track with no extra energetic clusters.¹⁰ The insert shows the signal region for $D^+ \rightarrow \mu\nu_\mu$ enlarged; the defined signal region is shown between the two arrows.

Table 2: Results for $\mathcal{B}_{\phi\pi} \equiv \mathcal{B}(D_s \rightarrow \mu^+\nu_\mu)$, $\mathcal{B}(D_s \rightarrow \tau^+\nu_\tau)$, and $f_{D_s^+}$. (Numbers have been updated using D_s lifetime of 0.50 ps.) Results below the line have not been used in this average from Ref. (15). The assumed value of $\mathcal{B}(D_s^+ \rightarrow \phi\pi^+)$ is listed whenever available. ALEPH average their two results to obtain a value for $f_{D_s^+}$.

Exp.	Mode	$\mathcal{B}(x10^3)$	$\mathcal{B}_{\phi\pi}(\%)$	$f_{D_s^+}$ (MeV)
CLEO-c	$\mu^+\nu_\mu$ (34)	$5.94 \pm 0.66 \pm 0.31$		$264 \pm 15 \pm 7$
CLEO-c	$\tau^+\nu_\tau$ (34)	$80.0 \pm 13.0 \pm 4.0$		$310 \pm 25 \pm 8$
CLEO-c	$\tau^+\nu_\tau$ (35)	$61.7 \pm 7.1 \pm 3.6$		$275 \pm 10 \pm 5$
CLEO-c	combined			$274 \pm 10 \pm 5$
Belle	$\mu^+\nu_\mu$ (36)	$6.44 \pm 0.76 \pm 0.52$		$279 \pm 16 \pm 12$
Average				275 ± 10
CLEO (37)	$\mu^+\nu_\mu$	$6.2 \pm 0.8 \pm 1.3 \pm 1.6$	3.6 ± 0.9	$273 \pm 19 \pm 27 \pm 33$
BEATRICE (38)	$\mu^+\nu_\mu$	$8.3 \pm 2.3 \pm 0.6 \pm 2.1$	3.6 ± 0.9	$312 \pm 43 \pm 12 \pm 39$
ALEPH (39)	$\mu^+\nu_\mu$	$6.8 \pm 1.1 \pm 1.8$	3.6 ± 0.9	$282 \pm 19 \pm 40$
ALEPH (39)	$\tau^+\nu_\tau$	$58 \pm 8 \pm 18$		
L3 (40)	$\tau^+\nu_\tau$	$74 \pm 28 \pm 16 \pm 18$		$299 \pm 57 \pm 32 \pm 37$
OPAL (41)	$\tau^+\nu_\tau$	$70 \pm 21 \pm 20$		$283 \pm 44 \pm 41$
BaBar (28)	$\mu^+\nu_\mu$	$6.74 \pm 0.83 \pm 0.26 \pm 0.66$	4.71 ± 0.46	$283 \pm 17 \pm 7 \pm 14$

Table 3: Summary of recent absolute branching fraction measurements of exclusive D^+ and D^0 semileptonic decays. When only the CLEO-c absolute number is available, no average number is provided.

Decay mode	B(%) [CLEO-c](31)	B(%) [BES](32)	B(%) [PDG06 average]
$D^0 \rightarrow K^- e^+ \nu_e$	$3.44 \pm 0.10 \pm 0.10$	$3.82 \pm 0.40 \pm 0.27$	3.47 ± 0.13
$D^0 \rightarrow \pi^- e^+ \nu_e$	$0.262 \pm 0.025 \pm 0.008$	$0.33 \pm 0.13 \pm 0.03$	
$D^0 \rightarrow K^{*-} e^+ \nu_e$	$2.16 \pm 0.15 \pm 0.08$		
$D^0 \rightarrow \rho^- e^+ \nu_e$	$0.194 \pm 0.039 \pm 0.013$		
$D^+ \rightarrow K^0 e^+ \nu_e$	$8.71 \pm 0.38 \pm 0.37$	$8.95 \pm 1.59 \pm 0.67$	8.7 ± 0.5
$D^+ \rightarrow \pi^0 e^+ \nu_e$	$0.44 \pm 0.06 \pm 0.003$		
$D^+ \rightarrow \bar{K}^{*0} e^+ \nu_e$	$5.56 \pm 0.27 \pm 0.23$		
$D^+ \rightarrow \rho^0 e^+ \nu_e$	$0.21 \pm 0.04 \pm 0.01$		
$D^+ \rightarrow \omega e^+ \nu_e$	$0.16_{-0.06}^{+0.07} \pm 0.01$		

Table 4: Fit parameters in Eq. (8), decay rates and CKM matrix elements. The first errors are statistical; the second systematic.²⁴

P	F	α	β
π	$0.64(3)(6)$	$0.44(4)(7)$	$1.41(6)(13)$
K	$0.73(3)(7)$	$0.50(4)(7)$	$1.31(7)(13)$

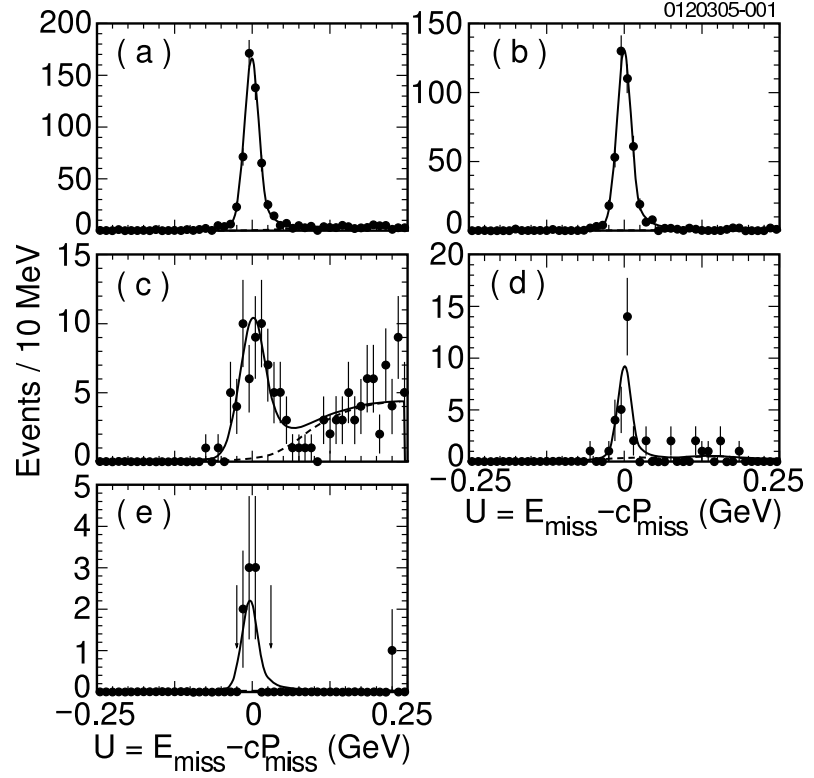


Figure 2: Fits (solid lines) to the U distributions in CLEO-c²⁸ data (dots with error bars) for the five D^+ semileptonic modes: (a) $D^+ \rightarrow \bar{K}^0 e^+ \nu_e$, (b) $D^+ \rightarrow \bar{K}^{*0} e^+ \nu_e$, (c) $D^+ \rightarrow \pi^0 e^+ \nu_e$, (d) $D^+ \rightarrow \rho^0 e^+ \nu_e$, (e) $D^+ \rightarrow \omega e^+ \nu_e$. The arrows in (e) show the signal region. The background (in dashed lines) is visible only in (c) and (d).

Table 5: Measured shape parameter α compared to lattice QCD predictions.

$\alpha(D^0 \rightarrow K \ell \nu)$	
Lattice QCD (12)	$0.5 \pm 0.04 \pm 0.07$
FOCUS (51)	$0.28 \pm 0.08 \pm 0.07$
CLEOIII (54)	$0.36 \pm 0.10^{+0.03}_{-0.07}$
Belle (7)	$0.52 \pm 0.08 \pm 0.06$
BaBar (53)	$0.38 \pm 0.02 \pm 0.03$
$\alpha(D^0 \rightarrow \pi \ell \nu)$	
Lattice QCD (12)	$0.44 \pm 0.04 \pm 0.07$
CLEO III (54)	$0.37^{+0.20}_{-0.31} \pm 0.15$
Belle (7)	$0.10 \pm 0.21 \pm 0.10$

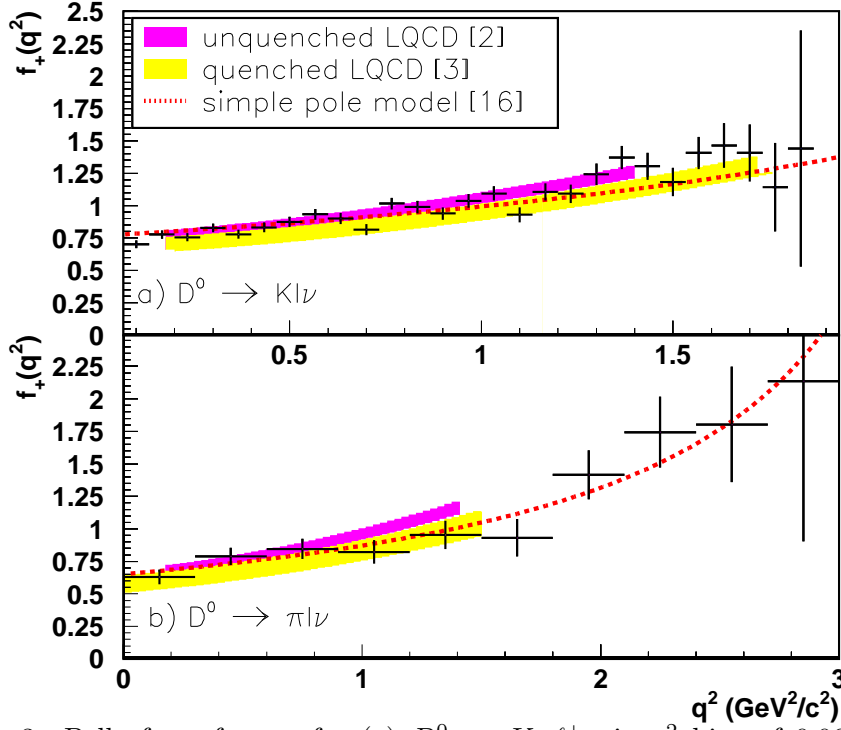


Figure 3: Belle form factors for (a) $D^0 \rightarrow K^- \ell^+ \nu$ in q^2 bins of 0.067 GeV^2 and (b) $D^0 \rightarrow \pi^- \ell^+ \nu$ in q^2 bins of 0.3 GeV^2 . Overlaid are the predictions of the simple pole model using the physical pole masses (dashed) and a quenched (yellow) and unquenched (purple) LQCD calculations. The shaded bands reflect the theoretical uncertainties and are shown in the q^2 ranges for which calculations are reported. (7).

Table 6: Representative predictions for flavor changing neutral current charm decays and experimental upper limits.

Decay Mode	LD ($\times 10^6$)	MSSMR ($\times 10^6$)	Experiment (90 % CL ul $\times 10^6$)
$D^+ \rightarrow \pi^+ e^+ e^-$	2.0 (63)	0.21(63) – 2.0(62)	7.4(64) 11.2 (67)
$D^+ \rightarrow \pi^+ \mu^+ \mu^-$	1.9	6.5(63) – 15(62)	24.4(67) 3.9(68)
$D^+ \rightarrow \pi^+ \mu^+ e^+$	0	30(62)	10.8(67)
$D^0 \rightarrow e^+ e^-$	1.0×10^{-17}	1.0×10^{-4}	1.2(69)
$D^0 \rightarrow \mu^+ \mu^-$	3.0×10^{-7}	3.5	1.3(69) 2.5 (70)
$D^0 \rightarrow \rho^0 e^+ e^-$	1.8	5.1	100.0 (71)

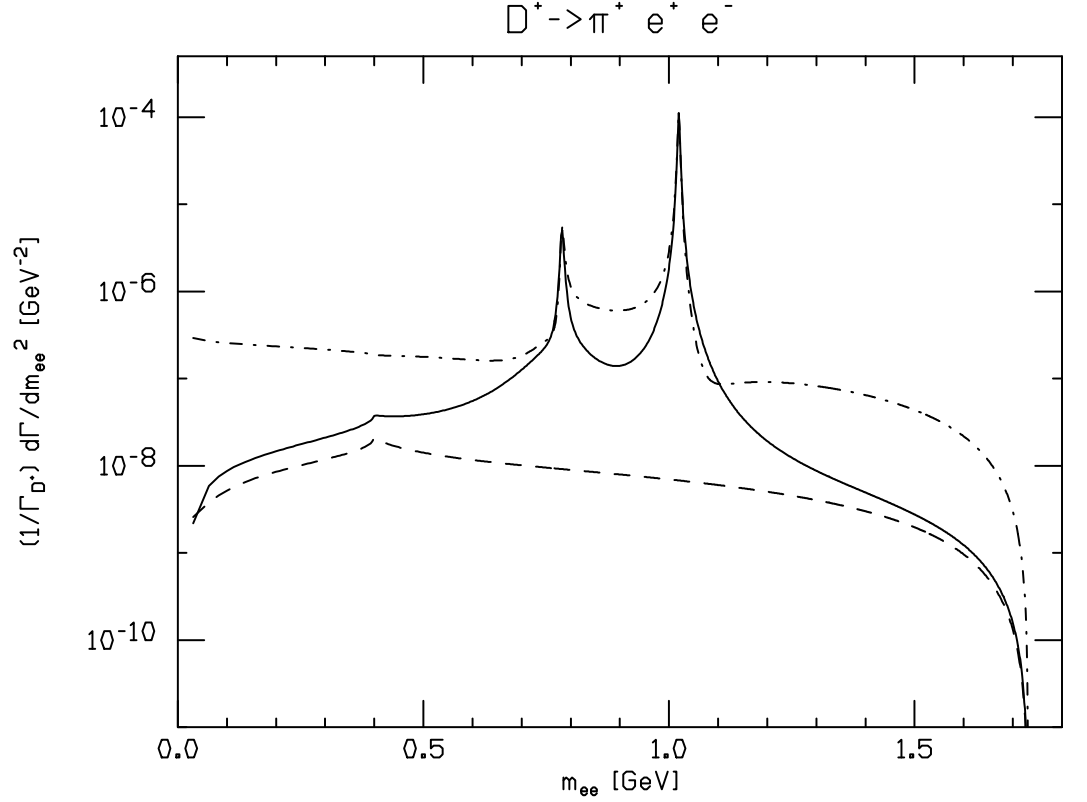


Figure 4: The dilepton mass distribution for $D^+ \rightarrow \pi^+ e^+ e^-$ (normalized to Γ_{D^+}) in the MSSM with nonuniversal soft breaking effects. The solid line is the SM. (I) $M_{\tilde{g}} = M_{\tilde{q}} = 250$ GeV; (II) $M_{\tilde{g}} = 2 M_{\tilde{q}} = 500$ GeV; (III) $M_{\tilde{g}} = M_{\tilde{q}} = 1000$ GeV; (IV) $M_{\tilde{g}} = (1/2) M_{\tilde{q}} = 250$ GeV. Curves are from Ref. (62)

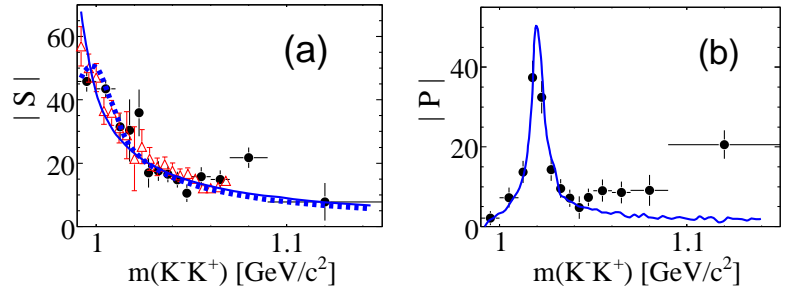


Figure 5: (a) The phase space corrected S -wave amplitude $|S|$ in the K^+K^- system, shown as black points, from $D^0 \rightarrow K^+K^-\pi^0$ decays. Red points are from an earlier analysis of $D^0 \rightarrow K^-K^+K_S^0$ decays. The solid blue curve is the line shape for $f_0(980)$ and the dotted curve for $a_0(980)$. In (b) are black points for $|P|$ from $D^0 \rightarrow K^+K^-\pi^0$ decays. The solid blue curve is the ϕ line shape. The figure is taken from Ref. (119).

Table 7: Recent absolute branching fraction data. For CLEO-c results, the uncertainty due to radiative corrections has been absorbed into the systematic uncertainty.

Mode	Absolute BF (%)	PDG(33) (%)
$D^0 \rightarrow K^- \pi^+$	$4.007 \pm 0.037 \pm 0.070$ (86)	3.82 ± 0.07
	$3.891 \pm 0.035 \pm 0.069$ (82)	
$D^0 \rightarrow K^- \pi^+ \pi^0$	$14.57 \pm 0.12 \pm 0.069$ (82)	
$D^0 \rightarrow K^- \pi^+ \pi^+ \pi^-$	$8.30 \pm 0.07 \pm 0.38$ (82)	
$D^+ \rightarrow K^+ \pi^+ \pi^+$	$9.14 \pm 0.10 \pm 0.17$ (82)	9.51 ± 0.34
$D^+ \rightarrow K^+ \pi^+ \pi^+ \pi^0$	$5.98 \pm 0.08 \pm 0.01$ (82)	6.00 ± 0.28
$D^+ \rightarrow K_S \pi^+$	$1.539 \pm 0.022 \pm 0.038$ (82)	1.47 ± 0.06
$D^+ \rightarrow K_S \pi^+ \pi^0$	$7.05 \pm 0.09 \pm 0.25$ (82)	7.0 ± 0.5
$D^+ \rightarrow K_S \pi^+ \pi^+ \pi^-$	$3.149 \pm 0.046 \pm 0.096$ (82)	3.11 ± 0.21
$D^+ \rightarrow K^+ K^- \pi^+$	$0.935 \pm 0.017 \pm 0.024$ (82)	1.0 ± 0.04
$D_s \rightarrow K^+ K^- \pi^+$	$5.50 \pm 0.23 \pm 0.16$ (83)	5.3 ± 0.8
	$4.0 \pm 0.4 \pm 0.4$ (87)	
$D_s \rightarrow K_S K^+$	$1.49 \pm 0.07 \pm 0.05$ (83)	2.2 ± 0.45
$D_s \rightarrow K^+ K^- \pi^+ \pi^0$	$5.62 \pm 0.33 \pm 0.51$ (83)	-
$D_s \rightarrow \pi^+ \pi^- \pi^+$	$1.11 \pm 0.07 \pm 0.04$ (83)	1.22 ± 0.23
$D_s \rightarrow \pi^+ \eta$	$1.47 \pm 0.12 \pm 0.14$ (83)	2.11 ± 0.35
$D_s \rightarrow \pi^+ \eta'$	$4.02 \pm 0.27 \pm 0.30$ (83)	4.7 ± 0.7

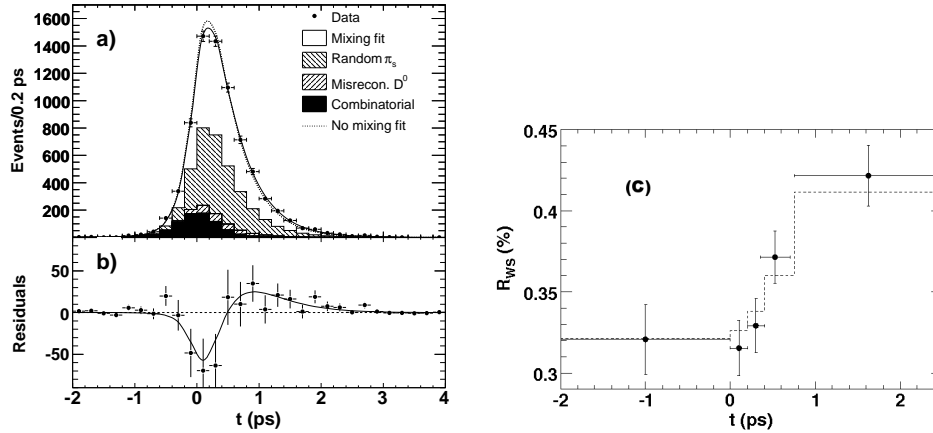


Figure 6: (a) Decay times for $D^0 \rightarrow K^+ \pi^-$ decays. The range includes negative values arising from measurement uncertainties. The solid curve is the result of the fit described in the text allowing for mixing and the dashed curve assumes no mixing ($x'^2 = y' = 0$). Contributions from various types of background are indicated. (b) Residuals of data bins from the fit with no mixing. The solid curve is the fit with mixing. (c) Ratio of WS to RS decays in time slices. The approximately linear form expected from Eq. 42 is evident in the data. Figures are from Ref. (124) (BaBar collaboration).

Table 8: Constraints on NP models from D^0 mixing.

Model	Approximate Constraint
Fourth Generation	$ V_{ub'}V_{cb'} \cdot m_{b'} < 0.5$ (GeV)
$Q = -1/3$ Singlet Quark	$s_2 \cdot m_S < 0.27$ (GeV)
$Q = +2/3$ Singlet Quark	$ \lambda_{uc} < 2.4 \cdot 10^{-4}$
Little Higgs	Tree: See entry for $Q = -1/3$ Singlet Quark Box: Region of parameter space can reach obser
Generic Z'	$M_{Z'}/C > 2.2 \cdot 10^3$ TeV
Family Symmetries	$m_1/f > 1.2 \cdot 10^3$ TeV (with $m_1/m_2 = 0.5$)
Left-Right Symmetric	No constraint
Alternate Left-Right Symmetric	$M_R > 1.2$ TeV ($m_{D_1} = 0.5$ TeV) $(\Delta m/m_{D_1})/M_R > 0.4$ TeV $^{-1}$
Vector Leptoquark Bosons	$M_{VLQ} > 55(\lambda_{PP}/0.1)$ TeV
Flavor Conserving Two-Higgs-Doublet	No constraint
Flavor Changing Neutral Higgs	$m_H/C > 2.4 \cdot 10^3$ TeV
FC Neutral Higgs (Cheng-Sher ansatz)	$m_H/ \Delta_{uc} > 600$ GeV
Scalar Leptoquark Bosons	See entry for RPV SUSY
Higgsless	$M > 100$ TeV
Universal Extra Dimensions	No constraint
Split Fermion	$M/ \Delta y > (6 \cdot 10^2$ GeV)
Warped Geometries	$M_1 > 3.5$ TeV
Minimal Supersymmetric Standard	$ (\delta_{12}^u)_{LR,RL} < 3.5 \cdot 10^{-2}$ for $\tilde{m} \sim 1$ TeV $ (\delta_{12}^u)_{LL,RR} < .25$ for $\tilde{m} \sim 1$ TeV
Supersymmetric Alignment	$\tilde{m} > 2$ TeV
Supersymmetry with RPV	$\lambda'_{12k}\lambda'_{11k}/m_{\tilde{d}_{R,k}} < 1.8 \cdot 10^{-3}/100$ GeV
Split Supersymmetry	No constraint

Table 9: Mixing and CPV parameters from $D^0 \rightarrow K^+\pi^-$ decays.

Fit Type	Parameter	Fit Results / 10^{-3}					
		BABAR(124)		CDF(147)		Belle(149)	
No CPV or mixing	R_D	3.53	\pm 0.09				3.77 \pm 0.01
	R_D	3.03	\pm 0.19	3.04	\pm 0.55	3.64	\pm 0.17
No CPV	x'^2	-0.22	\pm 0.37	-0.12	\pm 0.35	0.18	$^{+0.21}_{-0.23}$
	y'	9.7	\pm 5.4	8.5	\pm 7.6	0.6	$^{+4.0}_{-3.9}$
CPV allowed	R_D	3.03	\pm 0.19	-	-	-	-
	a_D	-21	\pm 54	-	-	23	\pm 47
	a_M	-	-	-	-	670	\pm 1200
	x'^{2+}	-0.24	\pm 0.52	-	-	< 0.72	
	x'^{2-}	-0.20	\pm 0.50	-	-	-	
	y'^+	9.8	\pm 7.8	-	-	-28	$< y' < 21$
	y'^-	9.6	\pm 7.5	-	-	-	

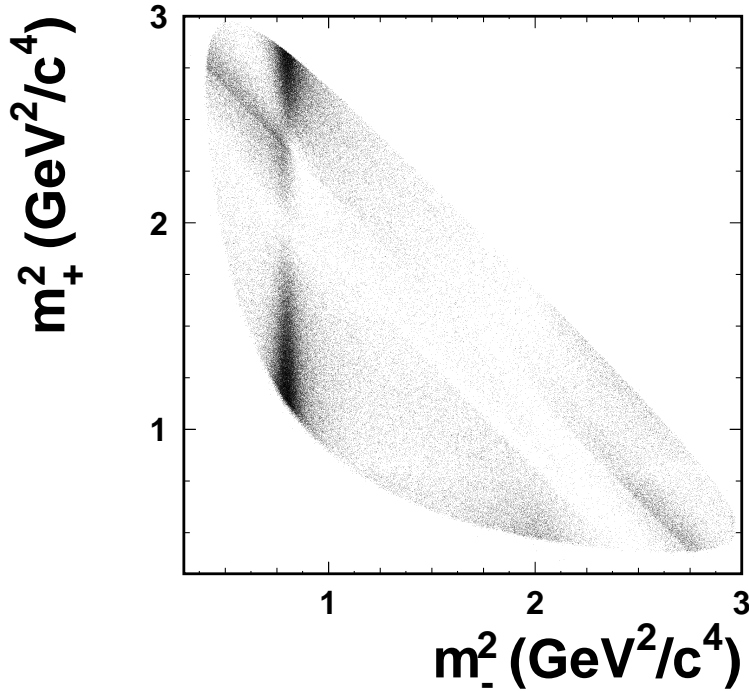


Figure 7: Dalitz plot of the decay $D \rightarrow K_S \pi^+ \pi^-$ showing squared invariant mass of $K_S \pi^+$ vs. that of $K_S \pi^-$ for data from Ref. (75) (Belle collaboration).

Table 10: Mixing and CPV parameters from $D^0 \rightarrow K_S \pi^+ \pi^-$ decays. The first uncertainty is statistical and the second systematic. The third is due to uncertainties in the isobar structure assumed in the model for the Dalitz plot distribution.

Fit Type	Parameter	Fit Result	95% C.L. Interval
No CP	$x(\%)$	$0.80 \pm 0.29^{+0.09}_{-0.07} +^{+10}_{-14}$	(0.0,1.6)
Violation	$y(\%)$	$0.33 \pm 0.24^{+0.08}_{-0.12} +^{+0.06}_{-0.08}$	(-0.34,0.96)
CP Viol.	$x(\%)$	$0.81 \pm 0.30^{+0.10}_{-0.07} +^{+0.09}_{-0.16}$	$ x < 1.6$
	$y(\%)$	$0.37 \pm 0.25^{+0.07}_{-0.13} +^{+0.07}_{-0.08}$	$ y < 1.04$
Allowed	$ q/p $	$0.86^{+0.30}_{-0.29} +^{+0.06}_{-0.03} \pm 0.08$	
	$\arg q/p$	$(-14^{+16}_{-18} +^{+5}_{-3} +^{+2}_{-4})^\circ$	
No direct	$ q/p $	$0.95^{+0.22}_{-0.20}$	
CP viol.	$\arg q/p$	$(-2^{+10}_{-11})^\circ$	

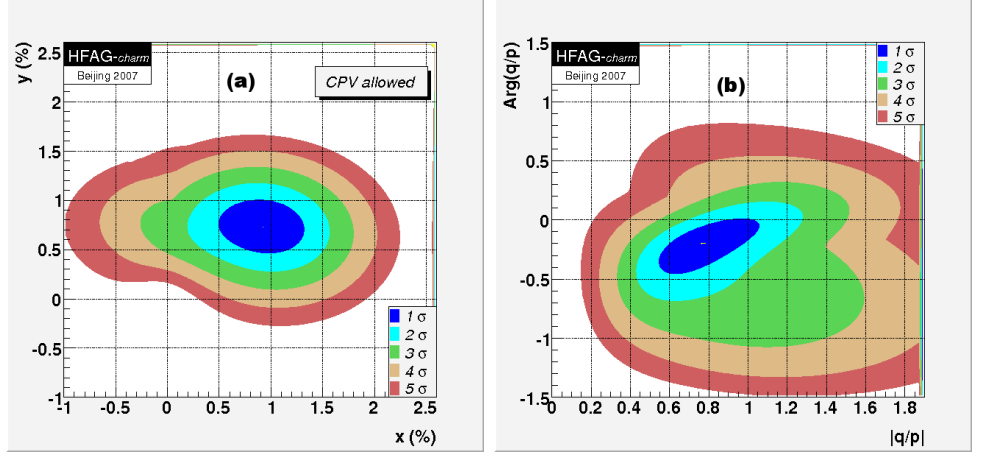


Figure 8: (a) Likelihood contours projected onto (x_D, y_D) plane from 8 parameter fit to 26 mixing observables for which data exists. (b) Projection onto the $(|p/q|, \arg p/q)$ plane for this fit.

Table 11: Asymmetries in decays of D mesons to various final states f . The asymmetry is defined in the text.

f	A_{CP} (%)	f	A_{CP} (%)
D^0 decays:		D^+ decays:	
Cabibbo Favored			
$K^-\pi^+$	-0.4 ± 1.0	$K_S\pi^+$	-0.9 ± 0.9
$K_S\pi^0$	$+0.1 \pm 1.3$	$K_S\pi^+\pi^0$	$+0.3 \pm 0.9$
$K^-\pi^+\pi^0$	$+0.2 \pm 0.9$	$K_S\pi^+\pi^-\pi^+$	$+0.1 \pm 1.3$
$K^-\pi^+\pi^-\pi^+$	$+0.7 \pm 1.0$	$K^-\pi^+\pi^+$	-0.5 ± 1.0
		$K^-\pi^+\pi^+\pi^0$	$+1.0 \pm 1.3$
Cabibbo Suppressed			
K^-K^+	$+0.15 \pm 0.34$	K_SK^+	$+7.1 \pm 6.2$
K_SK_S	-2.3 ± 1.9	$K^+K^-\pi^+$	$+0.6 \pm 0.8$
$\pi^-\pi^+$	$+0.02 \pm 0.51$	$K^+K^-\pi^+$	$+0.6 \pm 0.8$
$\pi^0\pi^0$	$+0.1 \pm 4.8$	$\pi^-\pi^+\pi^+$	-1.7 ± 4.2
$\pi^-\pi^+\pi^0$	$+0.1 \pm 5$	$K_SK^+\pi^-\pi^+$	-4.2 ± 6.8
$K^-K^+\pi^-\pi^+$	-8.2 ± 7.3		
$K_S\pi^+\pi^-$	$-0.9^{+2.6}_{-5.7}$		
Doubly Cabibbo Suppressed		Cabibbo Suppressed D_s	
$K^+\pi^-$	-0.8 ± 3.1	$D_s \rightarrow K^+\eta$	-20 ± 18
$K^+\pi^-\pi^0$	-0.1 ± 5.2	$D_s \rightarrow K^+\eta'$	-17 ± 37
$K^+\pi^-\pi^+\pi^-$	-1.8 ± 4.4	$D_s \rightarrow K_S\pi^+$	27 ± 11
		$D_s \rightarrow K^+\pi^0$	2 ± 29